RNA Biology

ISSN: 1547-6286 (Print) 1555-8584 (Online) Journal homepage: http://www.tandfonline.com/loi/krnb20

Superior cellular activities of azido- over amino-functionalized ligands for engineered preQ$_1$ riboswitches in *E.coli*

Eva Neuner, Marina Frener, Alexandra Lusser & Ronald Micura

To cite this article: Eva Neuner, Marina Frener, Alexandra Lusser & Ronald Micura (2018): Superior cellular activities of azido- over amino-functionalized ligands for engineered preQ$_1$ riboswitches in *E.coli*, RNA Biology, DOI: 10.1080/15476286.2018.1534526

To link to this article: https://doi.org/10.1080/15476286.2018.1534526

Publisher: Taylor & Francis

Journal: *RNA Biology*

DOI: 10.1080/15476286.2018.1534526

Superior cellular activities of azido- over amino-functionalized ligands for engineered preQ$_1$ riboswitches in *E.coli*

Eva Neuner, [a]† Marina Frener, [a]† Alexandra Lusser,*[b] and Ronald Micura*[a]

[a]*Institute of Organic Chemistry and Center for Molecular Biosciences Innsbruck CMBI, Leopold-Franzens University, Innrain 80-82, Innsbruck 6020, Austria.*

[b]*Division of Molecular Biology, Biocenter, Medical University of Innsbruck, Innrain 80-82, 6020 Innsbruck, Austria.*

† These authors contributed equally to this work

Corresponding authors: alexandra.lusser@i-med.ac.at, ronald.micura@uibk.ac.at

Superior cellular activities of azido- over amino-functionalized ligands for engineered preQ$_1$ riboswitches in *E.coli*

For this study, we utilized class-I and class-II preQ$_1$-sensing riboswitches as model systems to decipher the structure-activity relationship of rationally designed ligand derivatives *in vitro* and *in vivo*. We found that synthetic preQ$_1$ ligands with amino-modified side chains that protrude from the ligand-encapsulating binding pocket, and thereby potentially interact with the phosphate backbone in their protonated form, retain or even increase binding affinity for the riboswitches *in vitro*. They, however, led to significantly lower riboswitch activities in a reporter system *in vivo* in *E. coli*. Importantly, when we substituted the amino- by azido-modified side chains, the cellular activities of the ligands were restored for the class-I conditional gene expression system and even improved for the class-II counterpart. Kinetic analysis of ligand binding *in vitro* revealed enhanced on-rates for amino-modified derivatives while they were attenuated for azido-modified variants. This shows that neither high affinities nor fast on-rates are necessarily translated into efficient cellular activities. Taken together, our comprehensive study interconnects *in vitro* kinetics and *in vitro* thermodynamics of RNA-ligand binding with the ligands' *in vivo* performance and thereby encourages azido- rather than amino-functionalized design for enhanced cellular activity.

Keywords: RNA ligand recognition; modifications; riboswitches; kinetics; thermodynamics; RNA biosensor tools; preQ$_1$ derivatives

Introduction

Riboswitches have emerged as possible targets for the development of alternative antimicrobial approaches [1-8]. They are typically located in the 5' noncoding regions of bacterial mRNA and are able to bind specific metabolites to their aptamers with very high selectivity [9-11]. In a manner that is dependent on metabolite concentration, nascent mRNAs containing riboswitch domains can enter one of two mutually exclusive folding pathways to impart regulatory control [12]. The outcome of the folding pathway corresponds to ligand-bound or -free state. Thereby, the aptamer fold triggers structural cues into the expression platform which, in turn, transduces an "on" or "off" signal for gene expression, predominantly at the transcriptional or translational level [13-15].

One of the most critical steps in riboswitch gene regulation is ligand-sensing by the aptamer. For most riboswitches, the ligand becomes almost completely encapsulated by the RNA scaffold. Besides nucleobase stacking, most riboswitch aptamers involve every possible hydrogen donor or acceptor position of the ligand in hydrogen bond interactions with nucleotides of the binding pocket. This makes the structure-based design of modified ligand analogs and ligand mimics rather challenging. Nevertheless, the identification of novel potent ligands is a topic of intense research because ever since their discovery, riboswitches have been viewed as promising targets for the development of novel antibiotic strategies [16]. Likewise, efforts to engineer riboswitches for imaging purposes [17-19] or as biotechnological tools for the detection of endogenous and non-endogenous small molecules are in the focus of synthetic biologists interested in understanding and reprogramming cellular behavior [20].

In the present study, we examine the structure-activity relationships between 7-aminomethyl-7-deazaguanine ($preQ_1$) sensing riboswitches [21] and chemically functionalized $preQ_1$ ligands, both *in vitro* and *in vivo*. In particular, we ask the question how "add-on" functionalities such as aminoalkyl, azidoalkyl, and ethylene glycol moieties that can potentially interact with the phosphate backbone and that are amenable for further

derivatization, impact binding thermodynamics and kinetics and how the obtained *in vitro* parameters translate into riboswitch activity in the cell.

Results and discussion

Structure-based design of functionalized ligands for preQ$_1$-I and -II riboswitches

PreQ$_1$ is an intermediate of the biosynthesis pathway of the hypermodified nucleoside queuosine. Although queuosine is found in specific tRNAs of most eukaryotes and bacteria, it is only synthesized in bacteria. The queuosine modification enhances translational fidelity at the wobble position [22-25], and queuosine deficiency in bacteria can lead to reduced growth fitness and diminished virulence [26,27]. Bacterial riboswitches responsive to preQ$_1$ are currently known to fall into three phylogenetically distinct classes. The preQ$_1$-I (class 1) aptamer is distributed widely and rather compact, comprising not more than 34 nucleotides [28]. The preQ$_1$-II (class 2) riboswitch is about twice this size and has been found in the *Firmicutes* [29]. Both classes are prevalent among important pathogens, such as *Streptococcaceae*. By contrast, the preQ$_1$-III (class 3) riboswitch has been found exclusively in *Clostridium*, and it is the largest of all preQ$_1$ riboswitches [21].

In the present comprehensive study, we have focused on the two most widespread classes of preQ$_1$ riboswitches (I and II). These two classes employ distinct ligand binding modes (Figure 1) [30,31]. The class-I riboswitch recognizes preQ$_1$ with cytosine (C15) through classical Watson–Crick base pairing and additionally through bidentate interaction of the ligand's N3 and C2-NH$_2$ with the *trans* Watson–Crick face of adenosine (A29) (Figure 1A). Moreover, the N9-H of preQ$_1$ is H-bonding to the carbonyl O4 of uridine (U6) and the 7-aminomethyl moiety is involved in a further H-bond, namely to O6 of guanosine (G6).

The class-II riboswitch binds preQ$_1$ differently (Figure 1B). PreQ$_1$ pairs in bidentate fashion through *trans* Watson-Crick/Watson-Crick to cytidine (C30) and tridendate *via* N9-H–N3–C2-NH$_2$ to the *trans* Watson–Crick face of uridine (U41). The O6 of the preQ$_1$ lactam

moiety forms a water-mediated bridge to the 2'-OH of C30. Compared to the class-I riboswitch, the 7-aminomethyl group of the ligand is more strongly involved in interactions with the RNA, namely H-bonding to O6 of U31 and *via* electrostatic interactions to the phosphate group between A70 and A71.

Although $preQ_1$ binding modes of class I and II riboswitches are different with respect to H-bonding patterns, for both riboswitches the 7-aminomethyl group of the ligand remains solvent-accessible in the bound state. The 7-aminomethyl group therefore appears to be a suitable anchor for tether attachment without disturbing ligand-aptamer recognition. Because we intended to retain the interaction characteristics of the 7-aminomethyl moiety, its alkylation (resulting in secondary amines) rather than acylation (resulting in amides) was considered to provide the most fitting functionality for attachments.

For tethering additional functionalities to the native ligand, we have mainly focused on two types of modifications. *First*, aminoalkyl tethers as shown for derivative **3** and **4** (Figure 2) in their protonated form at suitable pH should be able to support binding of the modified ligand, based on specific electrostatic interactions with the phosphate backbone at the entrance of the ligand binding site. Higher affinities can be expected and additionally, binding kinetics are likely influenced due to an apparent increase in concentration because of non-specific interactions of the ammonium groups with the RNA phosphate backbone.

Second, azidoalkyl tethers as shown for derivative **5**, **6** and **7** (Figure 2) have been envisaged because of their potential for further straightforward functionalization with labeling compounds, e.g. fluorophores or biotin, using bioorthogonal Click or Staudinger reactions.

Moreover, we set out to analyze the impact of ethylene glycol moieties as shown for compound **8** (Figure 2). In a different context, earlier studies on oligoribonucleotide duplexes carrying this functionalization demonstrated a Mg^{2+}-chelating effect that can be utilized for enthalpic stabilization of RNA double helices [32]. We therefore speculated that this effect might be advantageous to stabilize small molecule–RNA interactions as well. Finally, we

wanted to analyze the binding properties of a ligand dimer **9** (Figure 2) that bridges two $preQ_1$ units via a short pentane linker to both 7-aminomethyl groups.

Synthesis of tethered $preQ_1$ ligands

To get access to the $preQ_1$ derivatives displayed in Figure 2, we have developed a robust protocol for reductive amination of 7-(aminomethyl)-7-deazaguanine **1** [33] and the corresponding phthalimido-protected aminoalkylaldehydes and azidoalkylaldehydes, respectively, using tetramethylammonium triacetoxyborohydride in dimethylformamide and acetic acid. The phthalimido group was then cleaved with aqueous hydrazine solution. All tethered $preQ_1$ derivatives were purified by reversed-phase chromatography applying an acetonitrile gradient to aqueous eluents containing one percent of trifluoroacetic acid. The products were thus obtained as salts of trifluoroacetic acid in excellent purity. Details of preparation are given in the Supporting Information. The developed routes provide significantly higher yields compared to direct alkylation of $preQ_1$ using bromoalkyl substrates [34].

Binding thermodynamics and kinetics of tethered $preQ_1$ ligands to class-I and -II riboswitches

Ligand affinities (K_D) as well as on-rates (k_{on}) for ligand binding were measured based on a fluorescence spectroscopic approach (Supporting Figure S1, Figure 3) that utilizes site-specifically 2-aminopurine (Ap) labeled RNA [35]. For $preQ_1$ class-I riboswitches, we focused on the specific aptamer sequence from *Thermoanaerobacter tengcongensis (Tte)*; for $preQ_1$ class-II riboswitches, we used the aptamer sequence from *Streptococcus pneumoniae (Spn)* (Figure 4). For both, suitable positions for Ap substitutions (U22Ap class I; A11Ap class II) have been identified [36-38].

Of note, the availability of the 7-aminomethyl group of native ligand **1** is particularly important for class-II riboswitches. Affinity was 7-fold reduced for ligand analog **2** (7-(3-aminopropyl)-7-deazaguanine; Supporting Figure S2A) that comprised an alkyl spacer placing

the amino group at greater distance from the ligand core (Figure 2); likely, the longer chain hinders positioning of the amino group to generate contacts to the phosphate of A70–A71 and to U31 in the RNA binding pocket.

Concerning the class-I $preQ_1$ riboswitch aptamer, the K_D values of amino- and azidopropyl and -butyl tethered ligands (**3** to **6**) measured in aqueous buffer at pH 7.5 (50 mM MOPS, 100 mM KCl, 293 K) in the presence of 2 mM $MgCl_2$ were comparable to native ligand **1**, varying only by a factor of 1.7 (Table 1, Figure 4, Supporting Figure S1 and S2). Ligands carrying longer chains, such as azidoethoxyethyl-$preQ_1$ **7** and triethylene glycol-linked $preQ_1$ **8**, experienced a 4-fold and 18-fold decrease in affinity, respectively (Table 1, Supporting Figure S2). We speculate that the conformational changes of the tethered group that are required for a chelating Mg^{2+} interaction (as indicated in Figure 1) might lead to an entropic destabilization that compensates the enthalpic stabilization. Also, for the $preQ_1$ dimer **9**, a loss in affinity (11-fold) was found (Table 1).

Interestingly, for the $preQ_1$ class-II riboswitch aptamer, the affinities measured for aminopropyl and -butyl tethered ligands (**3** and **4**) were increased by 3- to 4-fold compared to the native ligand, consistent with stabilizing interactions between the additional ammonium group and the RNA phosphate backbone at the entrance of the binding pocket (Table 2, Figure 4B, Supporting Figure S1B and S2A). In contrast to **3** and **4**, the K_D values of the corresponding azidopropyl and -butyl tethered ligands (**5** and **6**) were comparable to the native ligand, varying only by a factor of 1.7 (Table 2, Figure 4C, Supporting Figure S1C and S2A). Also, for azidoethoxyethyl-$preQ_1$ **7** the affinity remained comparable, however, the triethylene glycol-linked $preQ_1$ **8** and the $preQ_1$ dimer **9**, experienced a 10-fold and 4-fold loss in affinity, respectively (Table 2). From this *in vitro* analysis, it becomes obvious that varying affinities of a particular ligand derivative towards class-I and class-II aptamers likely originate from their distinct structural features leading to differential accomodation and interaction with the tether.

With regard to ligand binding kinetics, we note that previous studies have demonstrated that for the *Tte* class-I aptamer, $preQ_1$ binding kinetics are strongly dependent on $preQ_1$ concentrations [36]. Employing the U22Ap riboswitch variant for the 2ApFold fluorescence approach here, we determined an on-rate k_{on} of 11.3 x 10^3 $M^{-1}s^{-1}$ for $preQ_1$ **1** (Table 1). For the *Spn* class-II $preQ_1$ counterpart, however, we found that binding kinetics of $preQ_1$ **1** (based on the corresponding A11Ap variant) were independent of ligand concentration, with k_{obs} of 1.07±0.30 s^{-1} (over the same range of 2 to 14-fold excess of ligand over RNA as applied to the class-I counterpart). This suggests that a conformational change or conformational adaption of the class-II $preQ_1$ RNA is possibly rate-limiting for the ligand binding process.

For the aminoalkyl ligand derivatives **3** and **4** we found three to five-fold faster on-rates k_{on} for binding to the class-I aptamer compared to native $preQ_1$ **1** (Table 1, Figure 3, Supporting Figure S2B and S3). By contrast, the corresponding azidoalkyl ligands **5** and **6** with the same tether lengths were observed to have two and five-fold slower on-rates k_{on} than $preQ_1$ **1** for binding to the class-I aptamer (Table 1, Figure 3, Supporting Figure S2C). The faster on-rates for ligands **3** and **4** are consistent with the possibility for specific electrostatic interactions between the additional ammonium moieties and the phosphate backbone, and more generally, with an increase in local concentration due to improved electrostatic interactions with the negatively charged RNA. They are also consistent with an earlier proposed induced-fit binding mode of the $preQ_1$ class-I riboswitch [39,40].

Not unexpectedly, for the class-II riboswitch where ligand binding is not the rate limiting step but likely a conformational change that occurs in the RNA pocket, all $preQ_1$ ligand derivatives **3** to **9** exhibited rates k_{obs} that were comparable to that of the native ligand (Table 2, Figure 4, Supporting Figure S2 and S4). Only a slight rate difference among the ligand derivatives was observed, with azidobutyl modified $preQ_1$ **6** being slowest (k_{obs} 0.68±0.30 s^{-1}) and aminopropyl modified $preQ_1$ **3** together with dimer **9** being fastest (k_{obs}

1.05±0.16 s^{-1} and k_{obs} 1.06±0.11 s^{-1}) (Table 2, Supporting Figure S4). The here observed concentration-independence of class-II riboswitches with respect to binding rates is consistent with the conformational capture model that was deduced from NMR spectroscopic investigations [41]. This model proposed that stem P4 is poised to act as a "screw cap" on $preQ_1$ recognition to block ligand exit and stabilize the binding pocket.

Cellular activity of functionalized $preQ_1$ derivatives in a $preQ_1$ deficient E. coli strain

Previously, $preQ_1$ riboswitches have attracted attention as platforms for the engineering of orthogonal riboswitches to control gene expression. *Micklefield* and coworkers used a rational targeted approach in the evaluation of synthetic compounds with riboswitch mutants and identified an orthogonal riboswitch−ligand pair that effectively repressed the transcription of selected genes in *B. subtilis* [42]. More recently, rationally engineered $preQ_1$ riboswitches have been applied for inducible gene regulation in mycobacteria [43].

In this study, we investigated how the affinity and kinetic parameters obtained *in vitro* for functionalized $preQ_1$ derivatives (**2** to **9**) translate into cellular activity (Figure 4). We therefore engineered a $preQ_1$ class I or class II riboswitch- controlled reporter gene (green fluorescence protein, GFP) and monitored its production in response to the different ligands *in vivo* in *E. coli*. To avoid potential interference of endogenous $preQ_1$ with the assay, we used an *E. coli* strain bearing an inactivating mutation of the *queC* gene, which encodes a protein involved in the early steps of queuosine synthesis [44]. *Tte* and *Spn* $preQ_1$ riboswitches act at the level of translation by sequestering the Shine-Dalgarno sequence via ligand-triggered alternative RNA folding [21]. Successful binding of the $preQ_1$ ligand therefore results in a decrease of GFP production, which can be measured directly in the bacterial culture by determining GFP fluorescence. We used an inducible reporter system (pQE70 bacterial expression system) to repress GFP transcription in the absence of the inducer (IPTG) and added the different ligands concomitantly with the IPTG. Fluorescence measurements at 6 h after induction revealed that the native $preQ_1$ ligand **1** was capable of dose-dependent

regulation of class I–controlled GFP expression with an IC_{50} value of 27 μM and 75% repression observed at $preQ_1$ concentrations of 1 mM or higher (Figure 4A) while for the class II riboswitch, the IC_{50} value amounted to 96 μM with 65% repression at 1 mM or higher $preQ_1$ concentrations (Figure 4A).

We then evaluated the importance for *in vivo* activity of the native 7-aminomethyl group as a structural subunit in analogs of $preQ_1$ by measuring IC_{50} values of compound **2.** Although this compound comprises the 7-deazaguanine core, the replacement of the 7-aminomethyl by a 7-(3-aminopropyl) substituent renders it practically inactive *in vivo* regardless of the riboswitch tested (Supporting Figure S2A). This was especially surprising in the case of the class I riboswitch because *in vitro*, compound **2** displayed nearly the same affinity to class I aptamers as the native ligand.

Unexpectedly, the aminoalkylated ligands **3** and **4** that showed up to 4-fold higher affinities (class-II) and up to 5-fold increased on-rates (class-I) *in vitro* exhibited poor regulation ability *in vivo*. IC_{50} values for both riboswitch classes were at least 10-fold higher than those for native $preQ_1$ **1** (Table 1, Figure 4B, Supporting Figure S2B). However, when azido instead of amino groups were present at tethers of the same lengths, as in $preQ_1$ derivatives **5** and **6**, the *in vivo* activity was restored (for class I) or even improved (for class II) compared to the native $preQ_1$ **1** ligand (Table 1, Figure 4C, Supporting Figure S2C). Intriguingly, those ligands had shown significantly slower on-rates in *in vitro* binding studies (for class-I) (Figure 4C). Together, these findings demonstrate that azidoalkylated ligands exhibit excellent bioavailability and are potent triggers of riboswitch conformation changes resulting in the repression of translation *in vivo*. On the other hand, it appears that despite superior *in vitro* affinity of aminoalkylated ligands, they are less suitable for *in vivo* applications. Potential reasons for that could be reduced cellular uptake [45] or interference with polyamine metabolism in the cell [46].

We also tested the *in vivo* activity of azidoethoxyethyl $preQ_1$ derivative **7** and found that it was comparable to that of the native $preQ_1$ ligand for the class II riboswitch and slightly higher for the class I type (Figure 4D). The triethylene glycol modification of the ligand (derivative **8**) resulted in strongly decreased *in vitro* affinities of this ligand for both riboswitch classes. Interestingly, however, the *in vivo* activity of derivative **8** towards the class-II riboswitch was essentially equal to the native ligand (Supporting Figure S2D). For the class-I riboswitch, a similar trend was observed in that the decrease in IC_{50} value was less pronounced than expected considering its low affinity *in vitro* (Supplementary Figure S2D). Finally, the ligand dimer **9** showed clearly inferior *in vivo* activity towards both class-I and -II riboswitches compared to the native ligand **1** (Table 1 and 2).

Conclusions

For several reasons riboswitches have been considered attractive targets for antimicrobial drug development [1-5]: They are well structured and allow stable binding of low–molecular weight compounds to RNA with affinities as found for interactions between established antibiotics and ribosomal RNA. Furthermore, riboswitches have not been identified in mammals which should reduce the risk of undesired side effects. Finally, they are often located upstream of genes encoding enzymes that are involved in the synthesis of the metabolite that triggers the very riboswitch. By designing suitable metabolite analogs that outcompete the natural ligand for interaction with the riboswitch, the production of the metabolite will be inhibited by preventing the expression of the synthesis genes. If the respective metabolite is essential for life, this will lead to a growth stop and/or death of the bacterial cell. Several studies have demonstrated that riboswitches are indeed druggable [6-8,16,47-49]. The most prominent investigation employed a phenotypic screen and identified ribocil that acts as a structurally distinct mimic of the natural ligand flavin mononucleotide to repress *ribB* gene expression and inhibit cell growth [7].

Modest success, however, derived from ligand design that relied on the modulation of the nature and/or position of heteroatoms of the ligand core and/or the decoration of accessible positions with substituents that are typically used in medicinal chemistry as e.g. reported recently for guanine-sensing riboswitches in the bacterial pathogen *Clostridioides difficile* [6]. To the best of our knowledge, such studies have not yet included the evaluation of azide functionalization of ligands. Our study now demonstrates that the attachment of short azido-tethers to the native ligand of $preQ_1$ riboswitches leads to improved efficacy (> 2-fold decreased IC_{50}) and significantly increased repression (from 65% to 80%) of a GFP reporter in *E. coli*. These findings were unexpected because the thermodynamic and kinetic parameters k_{on} and K_D determined *in vitro* were clearly inferior to amino-modified derivatives and rather similar to the native ligand. It was furthermore unexpected that the amino-modified derivatives that gave the highest affinities *in vitro*, exhibited the lowest cellular activities of all $preQ_1$ derivatives investigated.

For future prospects, azido-modified $preQ_1$ ligands due to their excellent bioavailability and *in vivo* activity may constitute highly promising platforms for *in vivo* labeling approaches. The here presented azido-tethered $preQ_1$ derivatives are amenable for bioorthogonal labeling reactions with diverse reporter groups such as fluorophores. Recently, the structure-guided design of fluorescent *S*-adenosyl-L-methionine (SAM) analogs has been successfully introduced for a high throughput screen to target SAM-I riboswitch RNAs [50]. Such screens are likely expandable to $preQ_1$ riboswitches based on the derivatives presented. Finally, inspiration for live cell imaging applications of $preQ_1$-fluorophor conjugates can be drawn from a recent RNA imaging assay using the cobalamin riboswitch as an RNA tag and a series of probes containing the cobalamin ligand as a fluorescence quencher to elicit fluorescence turn-on upon binding RNA [17].

Disclosure of potential conflicts of interest

No potential conflicts of interest were disclosed.

Acknowledgments

We thank Roland Rokita for synthetic contributions to $preQ_1$ and Daniel Fellner for reagent synthesis for RNA solid-phase synthesis. We thank Christoph Kreutz for continuous NMR spectroscopic support. This work was supported by the Austrian Science Fund FWF [grant numbers I1040 to R.M., P27947 to R.M., P27024-BBL to A.L.], the Austrian Research Promotion Agency FFG [West-Austrian BioNMR 858017].

ORCID

Alexandra Lusser xxx

Ronald Micura http://orcid.org/0000-0003-2661-6105

References

1. Blount KF, Breaker RR. Riboswitches as antibacterial drug targets. Nat Biotechnol. 2006; 24:1558–64. doi:10.1038/nbt1268

2. Rekand IH, Brenk R. Ligand design for riboswitches, an emerging target class for novel antibiotics. Future Med Chem. 2017; 9:1649–62. doi:10.4155/fmc-2017-0063

3. Lünse CE, Schüller A, Mayer G. The promise of riboswitches as potential antibacterial drug targets. Int J Med Microbiol. 2014; 304:79–92. doi: 10.1016/j.ijmm.2013.09.002

4. Deigan KE, Ferré-D'Amaré AR. Riboswitches: discovery of drugs that target bacterial gene-regulatory RNAs. Acc Chem Res. 2011; 44:1329–38. doi: 10.1021/ar200039b

5. Groher F, Suess B. In vitro selection of antibiotic-binding aptamers. Methods. 2016; 106:42–50. doi:10.1016/j.ymeth.2016.05.008

6. Yan L-H, Le Roux A, Boyapelly K, Lamontagne A-M, Archambault M-A, Picard-Jean F, Lalonde-Seguin D, St-Pierre E, Najmanovich RJ, Fortier L-C, et al. Purine analogs targeting the guanine riboswitch as potential antibiotics against *Clostridioides difficile*. Eur J Med Chem. 2018; 143:755–68. doi:10.1016/j.ejmech.2017.11.079

7. Howe JA, Wang H, Fischmann TO, Balibar CJ, Xiao L, Galgoci AM, Malinverni JC, Mayhood T, Villafania A, Nahvi A, et al. Selective small-molecule inhibition of an RNA structural element. Nature. 2015; 526:672–7. doi:10.1038/nature15542

8. Dar D, Shamir M, Mellin JR, Koutero M, Stern-Ginossar N, Cossart P, Sorek R. Term-seq reveals abundant ribo-regulation of antibiotics resistance in bacteria. Science. 2016; 352:aad9822–2. doi:10.1126/science.aad9822

9. Breaker RR. Riboswitches and Translation Control. Cold Spring Harb Perspec Biol. 2018; doi:10.1101/cshperspect.a032797

10. Serganov A, Nudler E. A decade of riboswitches. Cell. 2013; 152:17–24. doi:10.1016/j.cell.2012.12.024

11. Batey RT. Riboswitches: still a lot of undiscovered country. RNA. 2015; 21:560–3. doi:10.1261/rna.050765.115

12. Haller A, Soulière MF, Micura R. The dynamic nature of RNA as key to understanding riboswitch mechanisms. Acc Chem Res. 2011; 44:1339–48. doi:10.1021/ar200035g

13. Lang K, Rieder R, Micura R. Ligand-induced folding of the thiM TPP riboswitch investigated by a structure-based fluorescence spectroscopic approach. Nucleic Acids Res. 2007; 35:5370–8. doi:10.1093/nar/gkm580

14. Uhm H, Kang W, Ha KS, Kang C, Hohng S. Single-molecule FRET studies on the cotranscriptional folding of a thiamine pyrophosphate riboswitch. Proc Natl Acad Sci USA. 2018; 115:331–6. doi: 10.1073/pnas.1712983115

15. Garst AD, Batey RT. A switch in time: Detailing the life of a riboswitch. BBA - Gene Regulatory Mechanisms. 2009; 1789:584–91. doi:10.1016/j.bbagrm.2009.06.004

16. Wang H, Mann PA, Xiao L, Gill C, Galgoci AM, Howe JA, Villafania A, Barbieri CM, Malinverni JC, Sher X, et al. Dual-Targeting Small-Molecule Inhibitors of the

Staphylococcus aureus FMN Riboswitch Disrupt Riboflavin Homeostasis in an Infectious Setting. Cell Chem Biol. 2017; 24:576–6. doi:10.1016/j.chembiol.2017.03.014

17. Braselmann E, Wierzba AJ, Polaski JT, ski MXACX, Holmes ZE, Hung S-T, Batan D, Wheeler JR, Parker R, Jimenez R, et al. A multicolor riboswitch-based platform for imaging of RNA in live mammalian cells. Nat Chem Biol. 2018; 14:1–11. doi:10.1038/s41589-018-0103-7

18. Kellenberger CA, Chen C, Whiteley AT, Portnoy DA, Hammond MC. RNA-Based Fluorescent Biosensors for Live Cell Imaging of Second Messenger Cyclic di-AMP. J Am Chem Soc. 2015; 137:6432–5. doi:10.1021/jacs.5b00275

19. Sunbul M, Jäschke A. SRB-2: a promiscuous rainbow aptamer for live-cell RNA imaging. Nucleic Acids Res. 2018; 6:331. doi:10.1093/nar/gky543

20. Sinha J, Reyes SJ, Gallivan JP. Reprogramming bacteria to seek and destroy an herbicide. Nat Chem Biol. 2010; 6:464–70. doi: 10.1038/nchembio.369

21. McCown PJ, Liang JJ, Weinberg Z, Breaker RR. Structural, Functional, and Taxonomic Diversity of Three $PreQ_1$ Riboswitch Classes. Chem Biol. 2014; 21:880–9. doi:10.1016/j.chembiol.2014.05.015

22. Hutinet G, Swarjo MA, de Crécy-Lagard V. Deazaguanine derivatives, examples of crosstalk between RNA and DNA modification pathways. RNA Biol. 2017; 14:1175–84. doi:10.1080/15476286.2016.1265200

23. Vinayak M, Pathak C. Queuosine modification of tRNA: its divergent role in cellular machinery. Biosci Rep. 2009; 30:135–48. doi:10.1042/BSR20090057

24. Bienz M, Kubli E. Wild-type tRNATyrG reads the TMV RNA stop codon, but Q base-modified tRNATyrQ does not. Nature. 1981; 294:188–90. doi:10.1038/294188a0

25. Yokoyama S, Miyazawa T, Iitaka Y, Yamaizumi Z, Kasai H, Nishimura S. Three-dimensional structure of hyper-modified nucleoside Q located in the wobbling position of tRNA. Nature. 1979; 282:107–9.

26. Noguchi S, Nishimura Y, Hirota Y, Nishimura S. Isolation and characterization of an Escherichia coli mutant lacking tRNA-guanine transglycosylase. Function and biosynthesis of queuosine in tRNA. J Biol Chem. 1982; 257:6544–50.

27. Durand JM, Okada N, Tobe T, Watarai M, Fukuda I, Suzuki T, Nakata N, Komatsu K, Yoshikawa M, Sasakawa C. vacC, a virulence-associated chromosomal locus of Shigella flexneri, is homologous to tgt, a gene encoding tRNA-guanine transglycosylase (Tgt) of Escherichia coli K-12. J Bacteriol. 1994; 176:4627–34. doi:10.1128/jb.176.15

28. Roth A, Winkler WC, Regulski EE, Lee BWK, Lim J, Jona I, Barrick JE, Ritwik A, Kim JN, Welz R, et al. A riboswitch selective for the queuosine precursor preQ1 contains an unusually small aptamer domain. Nat Struct Mol Biol. 2007; 14:308–17. doi:10.1038/nsmb1224

29. Meyer MM, Roth A, Chervin SM, Garcia GA, Breaker RR. Confirmation of a second natural preQ$_1$ aptamer class in *Streptococcaceae* bacteria. RNA. 2008; 14:685–95. doi:10.1261/rna.937308

30. Jenkins JL, Krucinska J, McCarty RM, Bandarian V, Wedekind JE. Comparison of a preQ$_1$ riboswitch aptamer in metabolite-bound and free states with implications for gene regulation. J Biol Chem. 2011; 286:24626–37. doi:10.1074/jbc.M111.230375

31. Liberman JA, Salim M, Krucinska J, Wedekind JE. Structure of a class II preQ$_1$ riboswitch reveals ligand recognition by a new fold. Nat. Chem. Biol. 2013; 9:353–5. doi:10.1038/nchembio.1231

32. Wu X, Pitsch S. Synthesis and pairing properties of oligoribonucleotide analogues containing a metal-binding site attached to beta-D-allofuranosyl cytosine. Nucleic Acids Res. 1998; 26:4315–23.

33. Levic J, Micura R. Syntheses of ^{15}N-labeled pre-queuosine nucleobase derivatives. Beilstein J Org Chem. 2014; 10:1914–8. doi:10.3762/bjoc.10.199

34. Ehret F, Zhou CY, Alexander SC, Zhang D, Devaraj NK. Site-Specific Covalent Conjugation of Modified mRNA by tRNA Guanine Transglycosylase. Mol Pharm. 2018; 15:737–42. doi:10.1021/acs.molpharmaceut.7b00356

35. Haller A, Altman RB, Soulière MF, Blanchard SC, Micura R. Folding and ligand recognition of the TPP riboswitch aptamer at single-molecule resolution. Proc Natl Acad Sci USA. 2013; 110:4188–93. doi:10.1073/pnas.1218062110

36. Frener M, Micura R. Conformational Rearrangements of Individual Nucleotides during RNA-Ligand Binding Are Rate-Differentiated. J Am Chem Soc. 2016; 138:3627–30. doi:10.1021/jacs.5b11876

37. Soulière MF, Haller A, Rieder R, Micura R. A Powerful Approach for the Selection of 2-Aminopurine Substitution Sites to Investigate RNA Folding. J Am Chem Soc. 2011; 133:16161–7. doi:10.1021/ja2063583

38. Soulière MF, Altman RB, Schwarz V, Haller A, Blanchard SC, Micura R. Tuning a riboswitch response through structural extension of a pseudoknot. Proc Natl Acad Sci USA. 2013; 110:E3256–64. doi:10.1073/pnas.1304585110

39. Suddala KC, Wang J, Hou Q, Walter NG. Mg(2+) shifts ligand-mediated folding of a riboswitch from induced-fit to conformational selection. J Am Chem Soc. 2015; 137:14075–83. doi:10.1021/jacs.5b09740

40. Suddala KC, Rinaldi AJ, Feng J, Mustoe AM, Eichhorn CD, Liberman JA, Wedekind JE, Al-Hashimi HM, Brooks CL, Walter NG. Single transcriptional and translational $preQ_1$ riboswitches adopt similar pre-folded ensembles that follow distinct folding pathways into the same ligand-bound structure. Nucleic Acids Res. 2013; 41:10462–75. doi:10.1093/nar/gkt798

41. Kang M, Eichhorn CD, Feigon J. Structural determinants for ligand capture by a class II preQ1 riboswitch. Proc Natl Acad Sci USA. 2014; 111:E663–71. doi: 10.1073/pnas.1400126111

42. Wu M-C, Lowe PT, Robinson CJ, Vincent HA, Dixon N, Leigh J, Micklefield J. Rational Re-engineering of a Transcriptional Silencing $PreQ_1$ Riboswitch. J Am Chem Soc. 2015; 137:9015–21. doi:10.1021/jacs.5b03405

43. Van Vlack ER, Topp S, Seeliger JC. Characterization of Engineered PreQ1 Riboswitches for Inducible Gene Regulation in Mycobacteria. J Bacteriol. 2017; 199: pii: e00656-16. doi:10.1128/JB.00656-16.

44. Gaur R, Varshney U. Genetic Analysis Identifies a Function for the queC (ybaX) Gene Product at an Initial Step in the Queuosine Biosynthetic Pathway in Escherichia coli. J Bacteriol. 2005; 187:6893–901. doi:10.1128/JB.187.20

45. Menzi M, Wild B, Pradère U, Malinowska AL, Brunschweiger A, Lightfoot HL, Hall J. Towards Improved Oligonucleotide Therapeutics Through Faster Target Binding Kinetics. Chem Eur J. 2017; 23:14221–30. doi:10.1002/chem.201701670

46. Bae D-H, Lane DJR, Jansson PJ, Richardson DR. The old and new biochemistry of polyamines. Biochim Biophys Acta. 2018; 1862:2053–68. doi:10.1016/j.bbagen.2018.06.004

47. Krajewski SS, Isoz I, Johansson J. Antibacterial and antivirulence effect of 6-N-hydroxylaminopurine in Listeria monocytogenes. Nucleic Acids Res. 2017; 45:1914–24. doi:10.1093/nar/gkw1308

48. Blount KF, Megyola C, Plummer M, Osterman D, O'Connell T, Aristoff P, Quinn C, Chrusciel RA, Poel TJ, Schostarez HJ, et al. Novel riboswitch-binding flavin analog that protects mice against Clostridium difficile infection without inhibiting cecal flora. Antimicrob Agents Chemother. 2015; 59:5736–46. doi:10.1128/AAC.01282-15

49. Mulhbacher J, Brouillette E, Allard M, Fortier L-C, Malouin F, Lafontaine DA. Novel Riboswitch Ligand Analogs as Selective Inhibitors of Guanine-Related Metabolic Pathways. PLoS Pathog. 2010; 6:e1000865. doi:10.1371/journal.ppat.1000865

50. Hickey SF, Hammond MC. Structure-Guided Design of Fluorescent *S*-Adenosylmethionine Analogs for a High-Throughput Screen to Target SAM-I Riboswitch RNAs. Chem Biol 2014; 21:345–56. doi: 10.1016/j.chembiol.2014.01.004

51. Hulme EC, Trevethick MA, Ligand binding assays at equilibrium: validation and interpretation. Brit J Pharmacol. 2010, 161, 1219-1237. doi:10.1016/0304-4165(80)90242-1

Table 1. Class-I preQ$_1$ riboswitches – Thermodynamic and kinetic parameters of ligand binding and cellular activity.

Ligand No.	K_D [nM]	k_{on} [$M^{-1}s^{-1}$ x10^{-3}]	k_{off} [s^{-1}] *	IC_{50} [µM] **
1	51	11.3	0.000576	27 (75%)
2	71	4.3	0.000305	n.d.
3	32	61.7	0.001974	>500
4	41	37.9	0.001554	>1000
5	30	4.6	0.000138	52 (65%)
6	88	2.5	0.000220	30 (70%)
7	167	2.4	0.000401	53 (42%)
8	922	3.4	0.003135	152 (56%)
9	590	3.5	0.002065	308 (38%)

* off-rates were calculated from $k_{off} = K_D \times k_{on}$ (ref. 51);

** number in brackets represents percentage of translational repression at saturating ligand concentration;

n.d. not detectable

Table 2. Class-II preQ$_1$ riboswitches – Thermodynamic and kinetic parameters of ligand binding and cellular activity.

Ligand No.	K_D [nM]	k_{obs} [s^{-1}]	k_{off} [s^{-1}] *	IC_{50} [µM] **
1	430	1.07	0.084733	96 (65%)
2	2830	>10***	n.d.	n.d.
3	97	1.05	0.019982	>500
4	148	0.80	0.022999	>1000
5	254	0.70	0.033841	71 (80%)
6	432	0.68	0.054080	40 (80%)
7	203	0.75	0.029262	92 (68%)
8	4580	0.72	0.031532	116 (65%)
9	1030	1.06	0.181061	328 (53%)

* off-rates were calculated from $k_{off} = k_{obs}/(1+([L]/K_D))$ (ref. 51);

** number in brackets represents percentage of repression at saturating ligand concentration;

*** estimated value;

n.d. not determined

Figure 1. Structural analyses of $preQ_1$ riboswitches. **A**) H-bond interactions between $preQ_1$ and RNA binding pocket of class-I riboswitch; **B**) H-bond interactions between $preQ_1$ and RNA binding pocket of class-II riboswitch; **C**) Three-dimensional structure of the *Thermoanaerobacter tengcongensis* (*Tte*) class-I $preQ_1$ riboswitch (PDB ID: 3Q50); **D**) Three-dimensional structure of the *Lactobacillus rhamnosus* class-II $preQ_1$ riboswitch (PDB ID: 4JF2); **E**) "Add-on" functionalities of $preQ_1$ ligands with the potential to interact with phosphate backbone units at the entrance of the ligand pocket to support ligand-RNA binding.

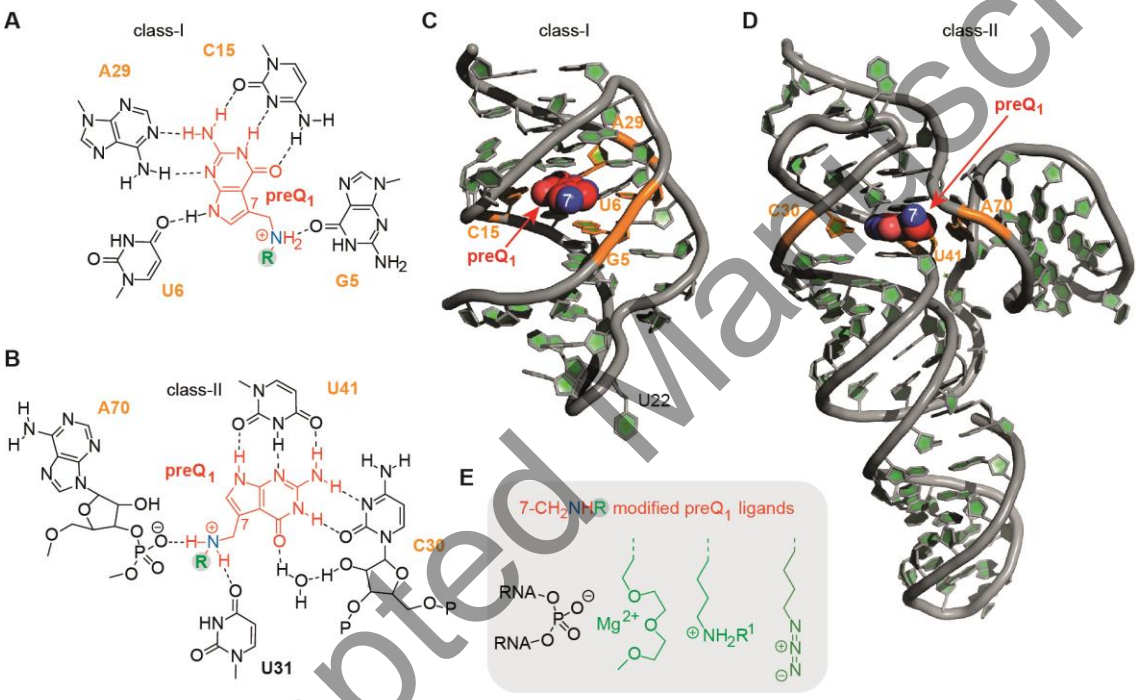

Figure 2. Chemical structures of the $preQ_1$ ligand derivatives synthesized for this study (for synthetic details see the Supporting Information).

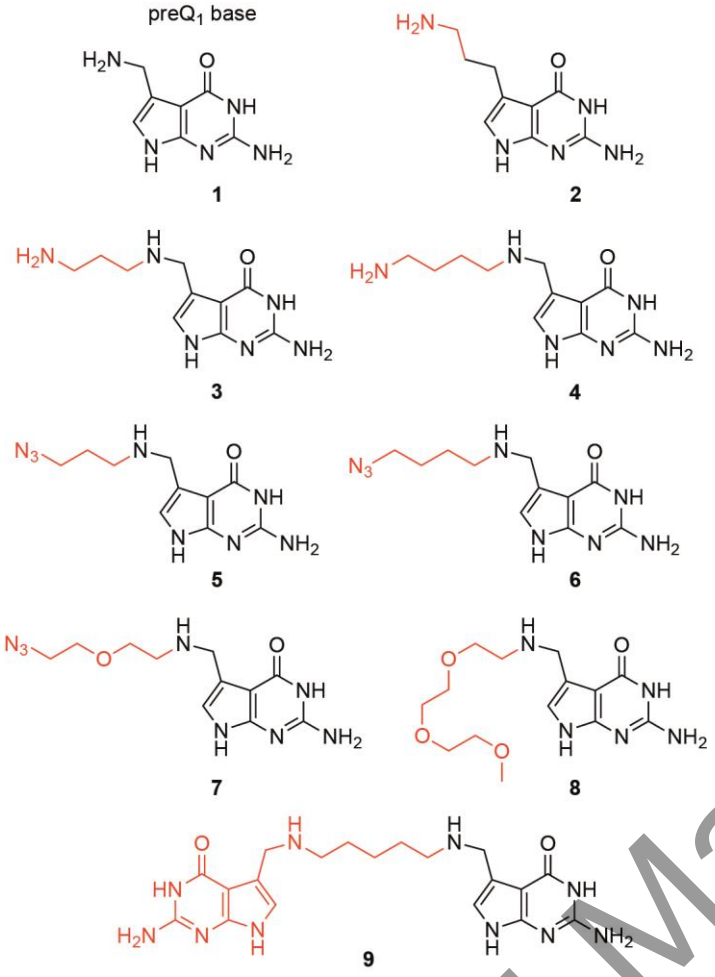

Figure 3. Stopped-flow fluorescence spectroscopy was used to monitor the kinetics of ligand $preQ_1$ binding to the *Tte* $preQ_1$ class-I riboswitch. **A**) Real time aminopurine (Ap) fluorescence time traces of the *Tte* U22Ap variant at different concentrations of 3-azidopropyl- and 4-azidobutyl-modified $preQ_1$ **5** and **6**; **B**) Rate constants k_{293} from plots of observed rate k_{obs} versus ligand concentration. **C**) Same as (**B**) but for the 3-aminopropyl and 4-aminobutyl-modified $preQ_1$ **3** and **4**. c(RNA) = 0.3 µM, c($MgCl_2$) = 2 mM, 100 mM KCl, 50 mM MOPS, pH 7.5, 293 K. Ligand concentration c(ligand) as indicated.

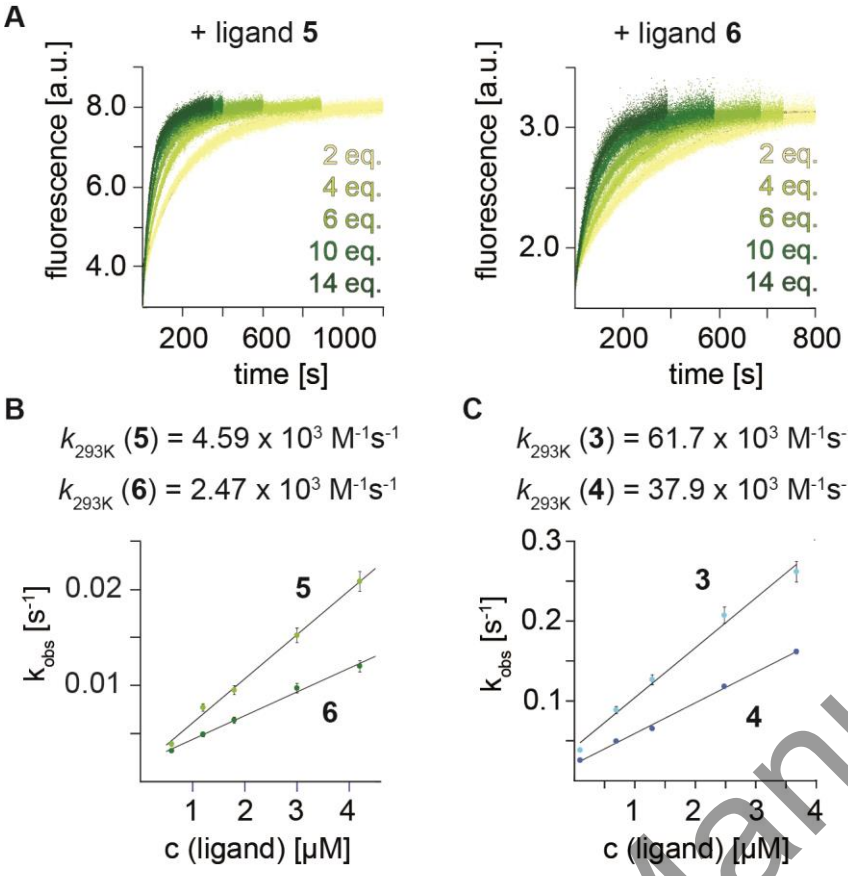

Figure 4. Comparison of *in vitro* and *in vivo* performance of $preQ_1$ class-I and -II riboswitches with $preQ_1$ and selected derivatives. **A**) Sequences of the *Tte* class-I (top left) and *Streptococcus pneumoniae* (*Spn*) class-II (top right) riboswitches used in this study. Nucleobase letters in black indicate the synthetic RNA aptamer sequences for K_D and k_{on} determinations (U22Ap and A11Ap substitution, respectively). Nucleobase letters in grey indicate the integration of the aptamers into the reporter mRNA. Letters in orange indicate nucleobases of the binding pocket that directly interact with the ligand via H-bonding. Exemplary fluorescence time traces of Ap-labeled $preQ_1$ RNAs in response to Mg^{2+} and $preQ_1$ ligand **1** (conditions: 0.5 µM RNA, 100 mM KCl, 50 mM MOPS, pH 7.5, 293 K. Ligands: 2 mM $MgCl_2$, 5 µM $preQ_1$ **1**); affinities K_D were obtained from plots of normalized AP fluorescence intensities plotted as a function of ligand concentrations (for details see Supporting Figure S1); rate constants $k_{on(293)}$ of the *Tte* $preQ_1$ class-I riboswitch were obtained

from plots of observed rates k_{obs} *vs* ligand concentrations (for details see Figure 3 and Supporting Figure S3); binding to the *Spn* $preQ_1$-II riboswitch was independent of ligand concentration; for details of k_{obs} determination see Supporting Figure S4. Dose-dependent repression of gene expression: B105 *E. coli* cells transformed with constructs expressing eGFP under translational control of $preQ_1$ class-I and -II riboswitches were assayed for eGFP fluorescence in the presence of different $preQ_1$ **1** concentrations (0.10 μM to 5 mM). Data represent the mean of three biological replicates, with error bars indicating standard deviation. The data were fit with a four-parameter logistic function to derive the IC_{50} values as indicated. **B**) Same as (**A**), but for ligand derivative **3**. **C**) Same as (**A**), but for ligand derivative **6**. **D**) Same as (**A**), but for ligand derivative **7**.

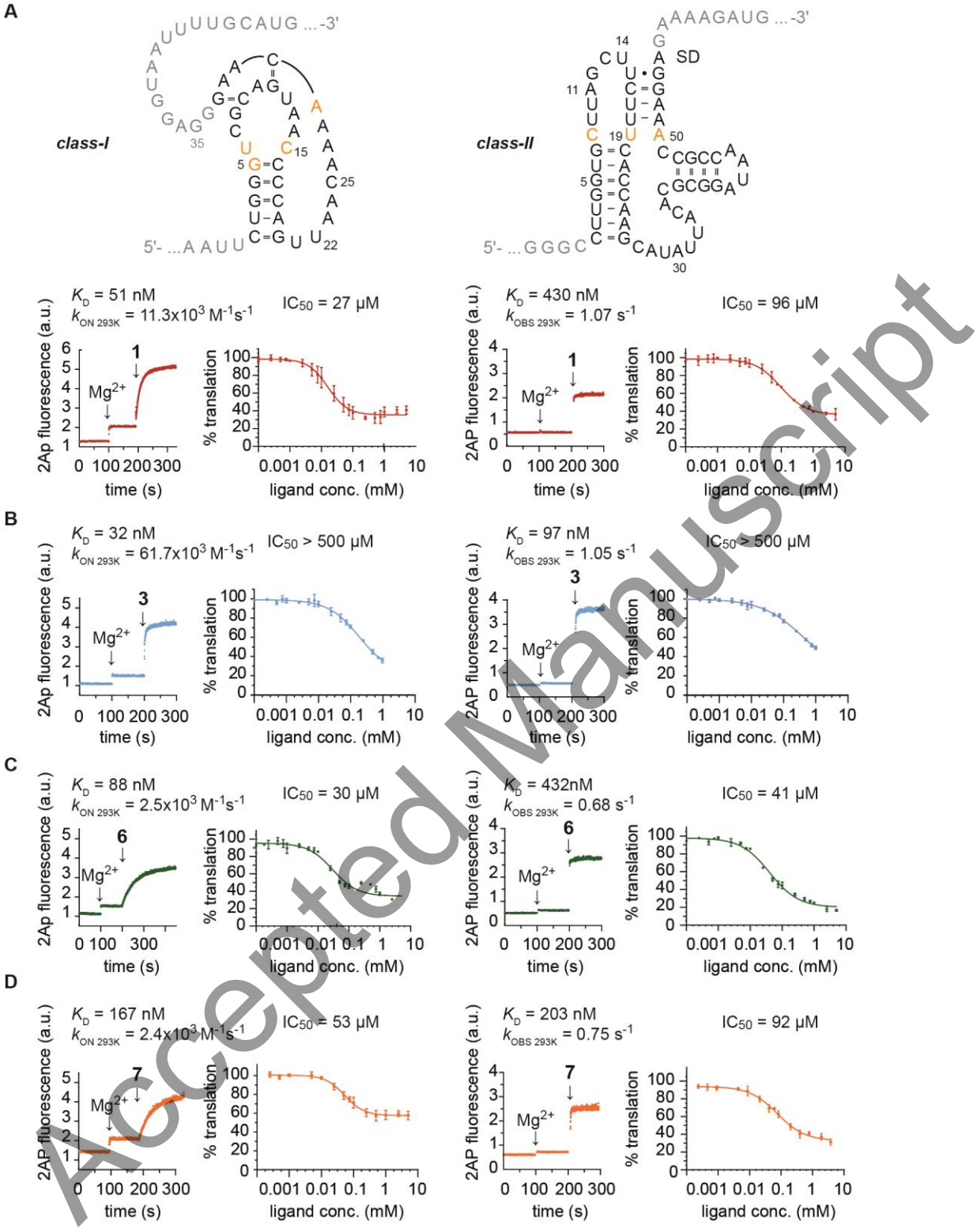

Supporting Information

Superior cellular activities of azido- over amino-functionalized ligands for engineered preQ$_1$ riboswitches in *E. coli*

Eva Neuner, Marina Frener, Alexandra Lusser, Ronald Micura

Contents

I. Supporting Methods

II. Supporting Figures

1. Synthesis of compound 2

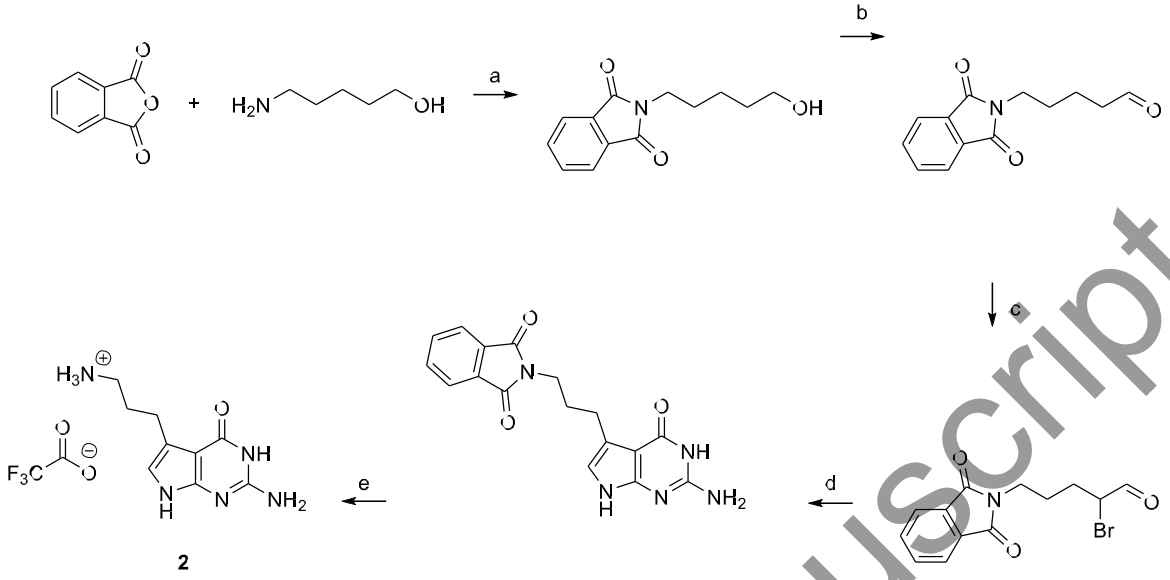

Scheme 1: Synthesis of compound **2**. a) Et_3N, toluene, reflux, 4 h, 81%. b) TCCA (1 eq), TEMPO, CH_2Cl_2, RT, 30 min., 58%. c) DBBA (0.6 eq), ACN, reflux, 4 h, 73%. d) 2,4-diaminopyrimidinone (1 eq), NaOAc (2 eq), H_2O/ACN, 40°C, 4 h, 58%. e) H_2NNH_2 (10 eq), EtOH, reflux, overnight, TFA (1%), RT, overnight, 83%.

1.1. N-(5-Hydroxypentyl)phthalimide

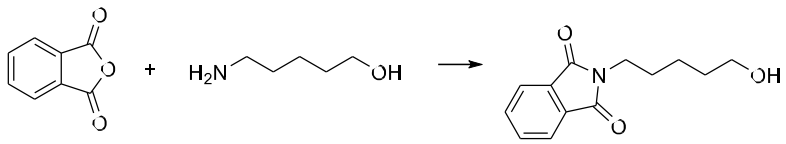

Aminopentanol (2.820 g, 27.3 mmol) was dissolved in tolune (41 ml) and phthalic anhydride (4.049 g, 27.3 mmol) and triethylamine (273 mg, 2.7 mmol) were added. The reaction mixture was heated to 130°C and refluxed for 4 hours. The solvents were evaporated, and the oily residue was dissolved in ethyl acetate. The organic phase was washed with 1 M HCl, saturated $NaHCO_3$ and saturated NaCl, dried over Na_2SO_4 and evaporated.

Yield: 5.158 g (81%) colorless oil

TLC (ethylacetate/cyclohexane, 1:1): *R_f = 0.32*

^{1}H-NMR (300 MHz, $CDCl_3$): δ 1.39 – 1.46 (m, 2H, H_2-C(3)); 1.57 – 1.76 (m, 4H, H_2-C(2), H_2-C(4)); 3.61 – 3.72 (m, 4H, H_2-C(1), H_2-C(5)); 7.71 (d, 2H, H-C(aromat.)); 7.83 (d, 2H, H-C(aromat.)) ppm.

1.2. N-(5-Oxopentyl)phthalimide

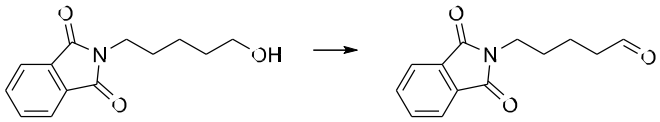

5-Hydroxypentylphthalimide (1.195 g, 5.12 mmol) was dissolved in dry dichloromethane (15 ml) and cooled to 0°C in an ice bath. Trichloroisocyanuric acid (1.190 g, 5.12 mmol) and 2,2,6,6-tetramethylpiperidinyloxyl (TEMPO) (8 mg, 0.0512 mmol) were added and a yellow suspension was formed. The reaction mixture was stirred at room temperature for 30 minutes and was then filtered through a celite pad. The organic phase was washed with saturated $NaHCO_3$, 1 M HCl and saturated NaCl, dried over Na_2SO_4, evaporated and dried under high vacuum.

Yield: 682 mg (58%) yellow oil

TLC (ethylacetate/cyclohexane, 1:1): $R_f = 0.5$

^{1}H NMR (300 MHz, $CDCl_3$): δ 1.66 – 1.76 (m, 4H, H_2-C(2), H_2-C(3)); 2.50 (t, 2H, H_2-C(4)); 3.71 (t, 2H, H_2-C(1)); 7.70 – 7.73 (m, 2H, H-C(arom.)); 7.83 – 7.86 (m, 2H, H-C(arom.)); 9.76 (s, 1H, HCO) ppm.

1.3. N-(4-Bromo-5-oxopentyl)phthalimide

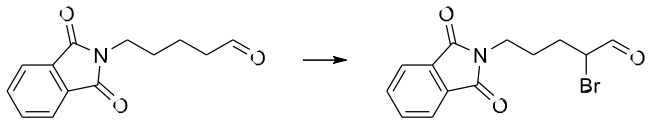

N-(5-oxopentyl)phthalimide (400 mg, 1.73 mmol) was dissolved in acetonitrile (5 ml) and 5,5-dibromobarbituric acid (297 mg, 1.03 mmol) was added. The solution was refluxed for 4 hours, cooled to room temperature and evaporated. The crude product was purified by column chromatography on silica gel (ethylacetate/cyclohexane, 2:8 – 3:7).

Yield: 392.6 mg (73%) colorless oil

TLC (ethylacetate/cyclohexane, 2:1): *R_f = 0.72*

^{1}H NMR (400 MHz, $CDCl_3$): δ 2.05 – 2.11 (m, 2H, H_2-C(2)); 2.46 – 2.50 (m, 2H, H_2-C(3)); 3.72 (t, 1H, H-C(4)); 3.78 (t, 2H, H_2-C(1)); 7.69 – 7.72 (m, 2H, H-C(arom.)); 7.81 – 7.84 (m, 2H, H-C(arom.)); 9.17 (1H, H-CO(5)) ppm.

1.4. 7-(3-Phthalimidopropyl)-7-deazaguanine

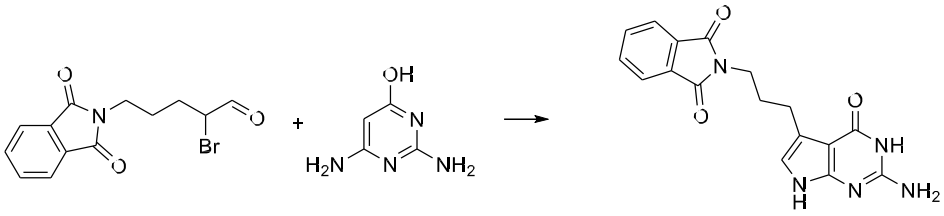

N-(4-Bromo-5-oxopentyl)phthalimide (390 mg, 1.6 mmol) was dissolved in water/acetonitrile (1/1) (5 ml) and 2,4-diaminopyrimidinone (159 mg, 1.26 mmol) and sodium acetate (207 mg, 2.52 mmol) were added. The reaction mixture was stirred at 40°C for 4 hours and the product started to precipitate after 40 minutes. The product was filtered off and dried under high vacuum.

Yield: 246 mg (58%) orange solid

TLC (ethylacetate/cyclohexane, 1:1): $R_f = 0$

^{1}H NMR (400 MHz, d_6-DMSO): δ 1.91 (t, 2H,); 2.58 (t, 2H,); 3.58 (t, 2H, H_2-C(1′)); 5.96 (2H, H_2-N(2)); 6.38 (1H, H-C(8)); 7.81-7.87 (m, 4H, H-C(arom.)); 10.09 (1H, H-N(1)); 10.62 (1H, H-N(9)) ppm.

1.5. 7-(3-Aminopropyl)-7-deazaguanine trifluoroacetate 2

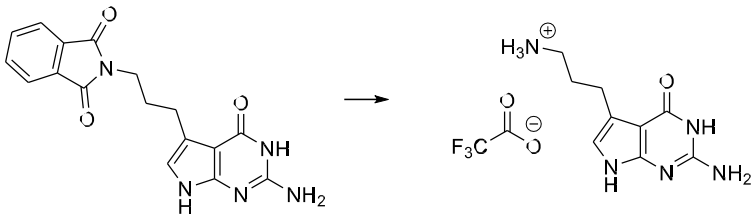

2

7-(3-Phthalimidopropyl)-7-deazaguanine (230 mg, 0.68 mmol) was dissolved in ethanol and hydrazine monohydrate (64%, 341 mg, 6.8 mmol) was added dropwise. The reaction mixture was refluxed overnight, the solvents were evaporated, and the crude product was dried under high vacuum. It was then suspended in trifluoroacetic acid (1%, 6 ml) and was shaken overnight at room temperature. The insoluble residue was filtered off and the filtrate was concentrated in vacuo. The crude product was purified by reversed phase chromatography on an ÄKTA prime plus system (LiChroprep® RP-18 (40 – 63 µm), 1% trifluoroacetic acid/acetonitrile, 100:0 – 70:30, 360 ml, flow rate 4 ml/min).

Yield: 182 mg (83%) of **2** as beige solid

HR-ESI-MS (m/z): $[M+H]^+$ calculated: [208.1193]; found: [208.1191]

^{1}H NMR (400 MHz, d_6-DMSO): δ 1.86 (2H, H_2-C(2′)); 2.63 (2H, H_2-C(1′)); 2.74 (2H, H_2-C(3′)); 6.19 (2H, H_2-N(2)); 6.43 (1H, H-C(8)); 7.68 (3H, H_3-N^+(3′)); 10.39 (1H, H-N(1)); 10.81 (1H, H-N(9)) ppm.

2. Synthesis of compound 3

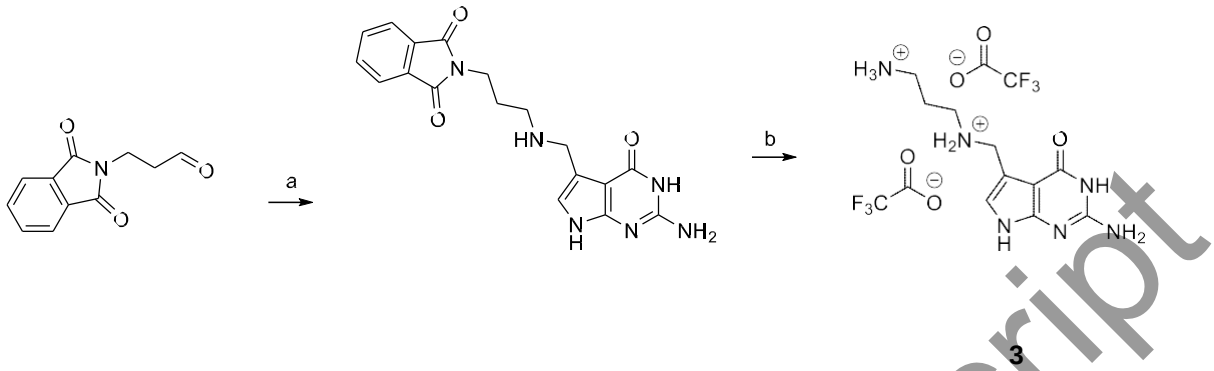

Scheme 2: Synthesis of compound **3**. a) $preQ_1$ (1.2 eq), $(CH_3)_4NHB(OAc)_3$ (2.5 eq), HOAc, DMF, RT, 5 h, 96%. b) H_2NNH_2 (10 eq), EtOH, reflux, overnight, TFA (1%), RT, overnight, 77%.

2.1. 7-((Phthalimidopropyl)aminomethyl)-7-deazaguanine

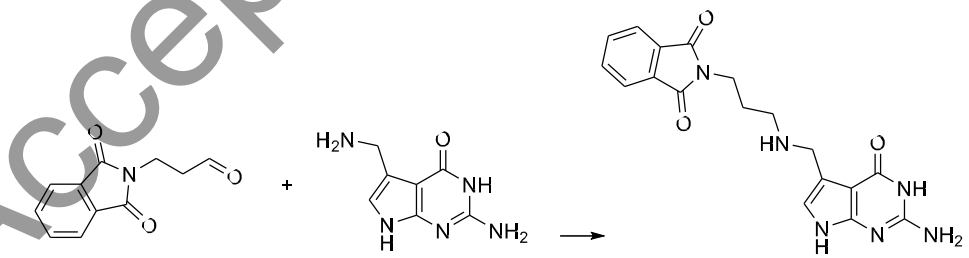

$PreQ_1$ (387 mg, 1.32 mmol) was dissolved in dimethylformamide (15 ml) and *N*-(3-oxopropyl)phthalimide (215 mg, 1.06 mmol) was added. After the successive addition of tetramethylammonium triacetoxyborohydride (697 mg, 2.65 mmol) and acetic acid (60 µl) the solution was stirred under argon at room temperature for 5 hours. The reaction mixture was concentrated in vacuo and the crude product was purified by column chromatography on silica gel (dichloromethane/methanol, 95:5 – 88:12).

Yield: 375 mg (96%) beige solid

TLC (dichloromethane/methanol, 85:15): *R_f = 0.33*

ESI-MS (m/z): $[M+H]^+$ calculated: [367.37], found: [367.15]

^{1}H NMR (300 MHz, d_6-DMSO): δ 1.98 (m, 2H, H_2-C); 2.99 (m, 2H, H_2-C); 3,65 (t, 2H, H_2-C); 4.13 (m, 2H, H_2-C(7)); 6.54 (s, 2H, H_2-N(2)); 6.80 (s, 1H, H-C(8)); 7.86 (d, 4H, H-C(arom.)); 9.23 (s, 1H, H-N(7)); 11.03 (s, 1H, H-N(1)); 11.27 (s, 1H, H-N(9)) ppm.

2.2. 7-((3-Aminopropyl)aminomethyl)-7-deazaguanine trifluoroacetate 3

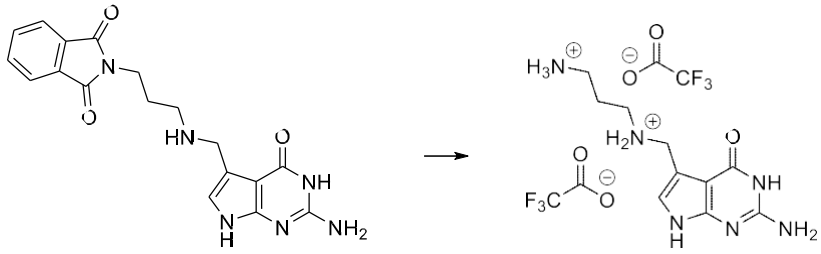

3

7-((Phthalimidopropyl)aminomethyl)-7-deazaguanine (375 mg, 1.02 mmol) was dissolved in ethanol (16 ml). Hydrazine monohydrate (64 %, 0.497 ml, 10.2 mmol) was added and the solution was refluxed overnight. The reaction mixture was concentrated in vacuo and the crude product was suspended in trifluoroacetic acid (1%, 20 ml) and shaken overnight at room temperature. The suspension was filtered off and the filtrate was concentrated in vacuo. The product was purified by reversed phase chromatography on an ÄKTA prime plus system (LiChroprep® RP-18 (40 – 63 µm), 1% trifluoroacetic acid/acetonitrile, 100:0 – 90:10, 360 ml, flow rate 4 ml/min).

Yield: 362 mg (77%) of **3** as beige solid

ESI-MS (m/z): $[M+H]^+$ calculated: [237.27], found: [237.29]

^{1}H NMR (300 MHz, d_6-DMSO): δ 1.91 (m, 2H, $H_2C(2')$); 2.87 (m, 2H, $H_2C(3')$); 3.01 (m, 2H, $H_2C(1')$); 4.17 (m, 2H, $H_2C(7)$); 6.40 (s, 2H, $H_2N(2)$); 6.83 (s, 1H, H-C(8)); 7.77 (m, 3H, ^+H_3N-C); 9.06 (m, 2H, ^+H_2N-C); 10.9 (s, 1H, H-N(9)); 11.3 (s, 1H, H-N(1)) ppm

3. Synthesis of compound 4

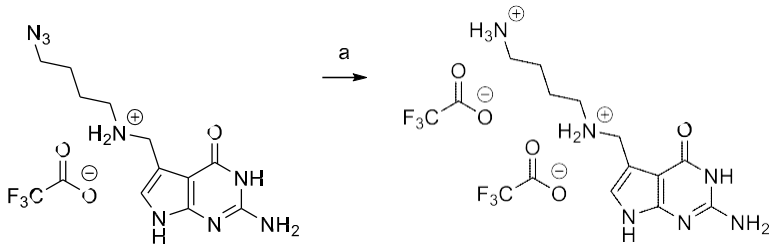

6 **4**

Scheme 3: Synthesis of compound **4**. a) Pd/C (10wt%), H_2, MeOH, RT, 3.5 h, 63%.

3.1. 7-((4-Aminobutyl)aminomethyl)-7-deazaguanine trifluoroacetate 4

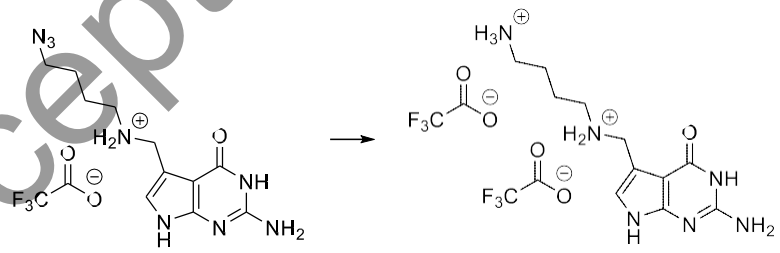

6 **4**

Azidobutyl-preQ$_1$ trifluroacetate (65 mg, 0.167 mmol) was dissolved in methanol (1.5 ml) and palladium on carbon (7.6 mg, loading 10wt%) was added. The suspension was stirred at room temperature and hydrogen in a balloon was bubbled through for half an hour. Afterwards the suspension was stirred under hydrogen atmosphere for 3 hours, diluted with methanol and filtered through a celite pad. The solution was concentrated in vacuo and the crude product was purified by reversed phase chromatography on an ÄKTA prime plus system (LiChroprep®

RP-18 (40 – 63 µm), 1% trifluoroacetic acid/acetonitrile, 95:5, flow rate 3 ml/min).

Yield: 50 mg (63%) of **4** as beige solid

ESI-MS (m/z): $[M+H]^+$ calculated: [251.32], found: [251.03]

^{1}H NMR (300 MHz, d_6-DMSO): δ 1.59 (m, 4H, H_2-C(2',3')); 2.97 (m, 2H, H_2-C(4')); 2.80 (m, 2H, H_2-C(1')); 4.16 (m, 2H, H_2-C(7)); 6.42 (s, 2H, H_2-N(2)); 6.83 (s, 1H, H-C(8)); 7.74 (m, 3H, $^+H_3$N-C); 9.03 (m, 2H, $^+H_2$N-C); 10.9 (s, 1H, H-N(9)); 11.3 (s, 1H, H-N(1)) ppm.

4. Synthesis of compound 5

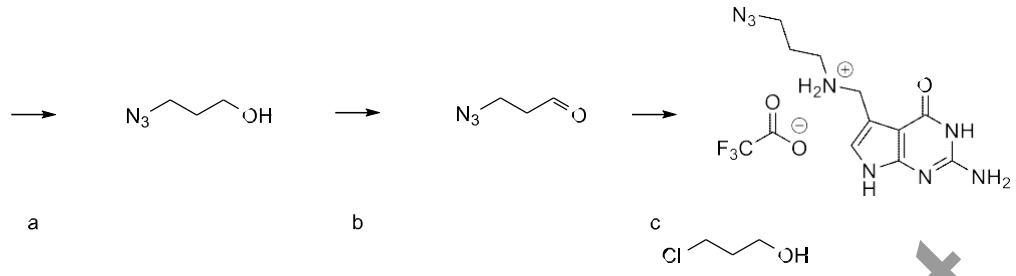

5

Scheme 4: Synthesis of compound **5**. a) NaN_3 (3 eq), DMF, 65°C, 22 h, 83%. b) Dess-Martin periodinane (1.3 eq), CH_2Cl_2, RT, 1 h, 92%. c) $preQ_1$ (1.1 eq), $(CH_3)_4NHB(OAc)_3$ (2 eq), HOAc, DMF, RT, 5 h, 47%.

4.1. 3-Azidopropanol

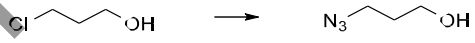

Sodium azide (4.68 g, 72 mmol) was suspended in dimethylformamide (16 m) and 3-chloropropanol (2 ml, 24 mmol) was added. The suspension was stirred under argon atmosphere for 22 hours at 65°C. After cooling to room temperature, the mixture was diluted with water, extracted with diethyl ether, washed with saturated $NaHCO_3$ and NaCl, dried over $MgSO_4$ and concentrated in vacuo.

Yield: 2.00 g (83%) colorless oil

TLC (pentane/diethyl ether, 75:25): *R_f = 0.18*

^{1}H NMR (300 MHz, d_6-DMSO): δ 1.66 (m, 2H, H_2-C(2)); 3.37 (m, 2H, H_2-C(1)); 3.46 (m, 2H, H_2-C(3));4.55 (t, 1H, OH) ppm.

4.2. 3-Azidopropanal

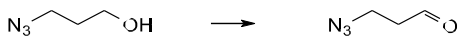

3-Azidopropanol (200 mg, 2.0 mmol) was dissolved in dry dichloromethane (20 ml) and Dess-Martin periodinane (1.10 g, 2.6 mmol) was added in portions. The reaction mixture was stirred for 1 hour at room temperature under argon atmosphere. Subsequently, the suspension was

filtered through a celite pad and the filtrate was concentrated in vacuo. The crude product was purified by column chromatography on silica gel (pentane/diethyl ether, 75:25).

Yield: 180 mg (92%) colorless oil

TLC (pentane/diethyl ether, 75:25): $R_f = 0.21$

^{1}H NMR (300 MHz, $CDCl_3$): δ 2.96 (t, 2H, H_2-C); 3.82 (t, 2H, H_2-C); 9.82 (d, 1H, H-CO) ppm.

4.3. 7-((3-Azidopropyl)aminomethyl)-7-deazaguanine trifluoroacetate 5

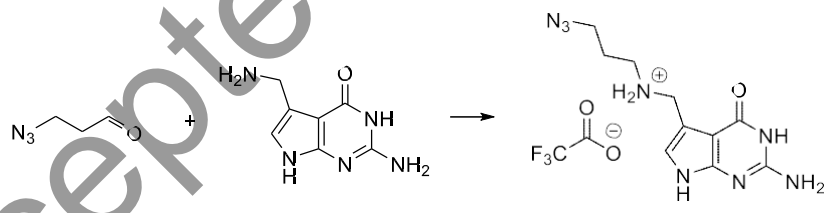

5

3- Azidopropanal (49 m, 0.49 mmol) was dissolved in dimethylformamide (10 ml) and $preQ_1$ trifluoroacetate (158 mg, 0.54 mmol) was added. After the addition of tetramethylammonium triacetoxyborohydride (258 mg, 0.98 mmol) and acetic acid (27 µl) the solution was stirred for 5 hours at room temperature. The reaction mixture was concentrated in vacuo and the crude product was purified by reversed phase chromatography on an ÄKTA prime plus system (LiChroprep® RP-18 (40 – 63 µm), 1% trifluoroacetic acid/acetonitrile, 100:0 – 70:30, 360 ml, flow rate 3 ml/min).

Yield: 87 mg (47%) of **5** as beige solid

ESI-MS (m/z): $[M+H]^+$ calculated: [263.28], found: [263.25]

^{1}H NMR (300 MHz, d_6-DMSO): δ 1.86 (m, 2H, $H_2C(2')$); 3.00 (m, 2H, $H_2C(3')$); 3.48 (m, 2H, $H_2C(1')$); 4.17 (m, 2H, $H_2C(7)$); 6.34 (s, 2H, $H_2N(2)$); 6.82 (s, 1H, H-C(8)); 8.94 (m, 2H, ^+H_2N-C(7)); 10.9 (s, 1H, H-N(9)); 11.3 (s, 1H, H-N(1)) ppm.

5. Synthesis of compound 6

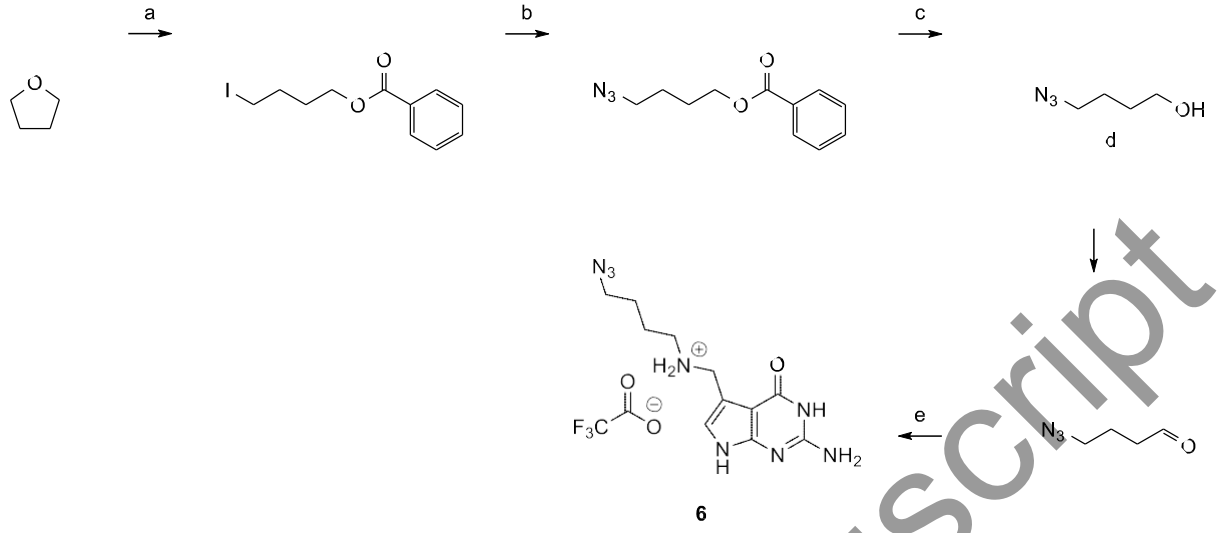

Scheme 5: Synthesis of compound **6**. a) NaI (1 eq), benzoyl chloride (1 eq), ACN, RT, overnight, 90%.

b) NaN_3 (1.5 eq), DMF, 0°C – RT, overnight, quantitative. c) LiOH (1.2 eq), THF/H_2O/MeOH (10/4/1.1), RT, overnight, 95%. d) Dess-Martin periodinane (1.3 eq), CH_2Cl_2, RT, 1 h, 86%. e) $preQ_1$ (1.1 eq), $(CH_3)_4NHB(OAc)_3$ (3.1 eq), HOAc, DMF, RT, 5 h, 46%.

5.1. 4-Iodobutyl benzoate[1]

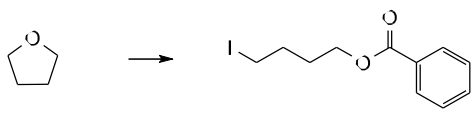

To a cooled solution of sodium iodide (18.4 g, 123 mmol) in tetrahydrofuran (10 ml, 123 mmol) and acetonitrile (5 ml), benzoyl chloride (14.8 ml, 123 mmol) was added in one portion. The reaction mixture was stirred in the dark overnight. After dilution of the reaction mixture with water and ether, the organic layers were separated and the aqueous layer was extracted three times with ether. The combined organic layers were washed with saturated $NaHSO_3$, Na_2CO_3 and dried over $MgSO_4$. The solvent was removed in vacuo to give the product as colorless oil.

Yield: 33.7 g (90%) colorless oil

^{1}H NMR (300 MHz, $CDCl_3$): δ 1.86-1.96 (m, 4H, 2x H_2-C); 3.22 (t, 2H, H_2-CO); 4.32 (t, 2H, H_2-Cl); 7.42 (t, 2H, H-C(arom.)); 7.52 (m, 1H, H-C(arom.)); 8.02 (m, 2H, H-C(arom.)) ppm.

5.2. 4-Azidobutyl benzoate[1]

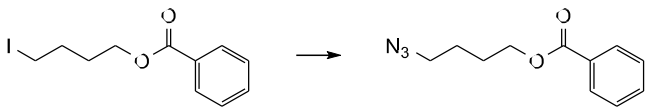

Sodium azide (5.89 g, 90.4 mmol) was added in portions to a solution of 4-iodobutyl benzoate (18.4 g, 60.2 mmol), in dimethylformamide (90 ml) in an ice bath in the dark. The reaction mixture was allowed to stir overnight and was subsequently diluted with ether and water. The organic layer was separated and the aqueous layer was further extracted with ether three times. The combined organic layers were concentrated in vacuo and the concentrate was diluted with hexane, washed with water and saturated NaCl, and dried over $MgSO_4$. The solvent was removed in vacuo to give the product as colorless oil.

Yield: 13.2 g (quantitative) colorless oil

^{1}H NMR (300 MHz, $CDCl_3$): δ 1.68-1.79 (m, 4H, 2x H_2-C); 3.27 (t, 2H, H_2-CN_3); 4.28 (t, 2H, H_2-CO); 7.37 (m, 2H, H-C(arom.)); 7.47 (m, 1H, H-C(arom.)); 8.00 (m, 2H, H-C(arom.)) ppm.

5.3. 4-Azidobutanol[1]

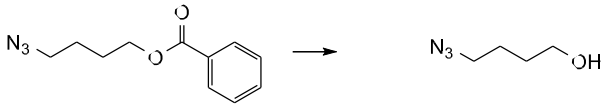

Lithium hydroxide (3.10 g, 74 mmol) was added to a solution of 4-azidobutyl benzoate (13.5 g, 61.6 mmol) in tetrahydrofuran (40 ml), water (16 ml) and methanol (4.4 ml). The reaction mixture was stirred overnight and subsequently diluted with water and ether. The layers were separated and the aqueous layer was further extracted with ether three times. The combined organic layers were washed with saturated NaCl and dried over $MgSO_4$. The solvent was removed in vacuo to give the product as yellow oil.

Yield: 6.73 g (95%) yellow oil

^{1}H NMR (300 MHz, $CDCl_3$): δ 1.72-1.56 (m, 4H, 2x H_2-C); 1.88 (s, 1H, OH); 3.31 (t, 2H, H_2-CN_3); 3.65 (t, 2H, H_2-COH) ppm.

5.4. 4-Azidobutanal

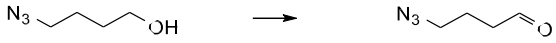

4- Azidobutanol (830 mg, 7.20 mmol) was dissolved in dry CH_2Cl_2 (70 ml) and Dess-Martin periodinane (3.97 g, 9.36 mmol) was added. The white suspension was stirred at room temperature under argon atmosphere. After 1 hour the mixture was diluted with dichloromethane, washed with saturated $Na_2S_2O_3$, $NaHCO_3$ and NaCl, dried over Na_2SO_4 and concentrated in vacuo. The crude product was purified by column chromatography on silica gel (diethyl ether/hexane, 25:75).

Yield: 697 mg (86%)

TLC (diethyl ether/hexane, 25:75): R_f = 0.21

^{1}H NMR (300 MHz, $CDCl_3$): δ 1.93 (m, 2H, H_2-C(2)); 2.60 (m, 2H, H_2-C(3)); 3.38 (m, 2H, H_2-C(1)); 9.82 (s, 1H, H-CO) ppm.

5.5. 7-((4-Azidobutyl)aminomethyl)-7-deazaguanine trifluoroacetate 6

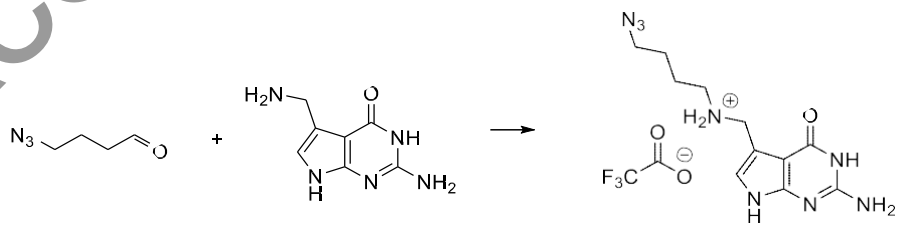

6

4-Azidobutanal (305 m, 2.70 mmol) was dissolved in dimethylformamide (30 ml) and $preQ_1$ trifluoroacetate (871 mg, 2.97 mmol) was added. After the addition of tetramethylammonium

triacetoxyborohydride (2.21 g, 8.40 mmol) and acetic acid (154 µl) the solution was stirred for 5 hours at room temperature under argon atmosphere. The reaction mixture was concentrated in vacuo and the crude product was purified by reversed phase chromatography on an ÄKTA prime plus system (LiChroprep® RP-18 (40 – 63 µm), 1% trifluoroacetic acid/acetonitrile, 100:0 – 70:30, 360 ml, flow rate 3 ml/min).

Yield: 486 mg (46%) of **6** as beige solid

TLC (RP, acetonitrile/TFA(1%), 1:1): *R_f = 0.66*

ESI-MS (m/z): $[M+H]^+$ calculated: [277.31]; found: [277.07]

^{1}H NMR (300 MHz, d_6-DMSO): δ 1.60 (m, 4H, H_2-C(2',3')); 2.98 (m, 2H, H_2-C(4')); 3.37 (m, 2H, H_2-C(1')); 4.16 (m, 2H, H_2-C(7)); 6.34 (s, 2H, H_2-N(2)); 6.82 (s, 1H, H-C(8)); 8.94 (m, 2H, $^+H_2$-NC(7)); 10.9 (s, 1H, H-N(9)); 11.3 (s, 1H, H-N(1)) ppm.

6. Synthesis of compound 7

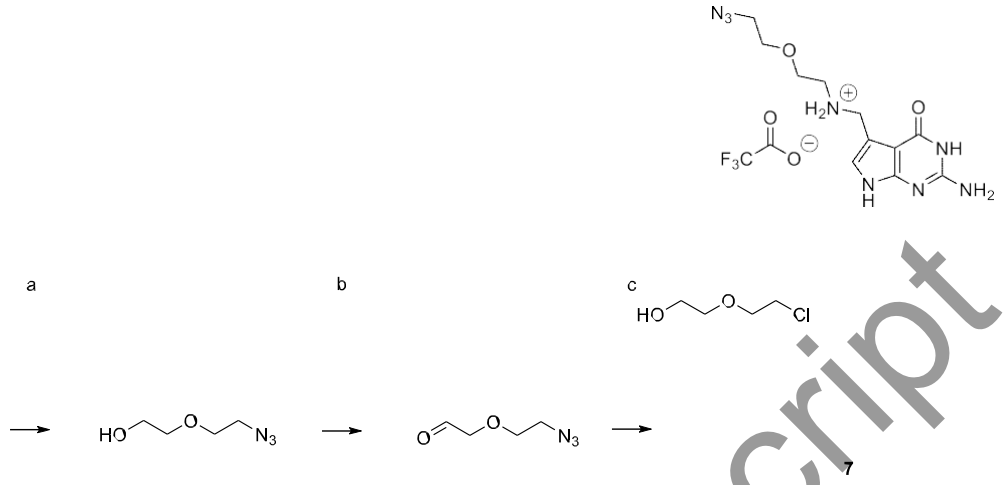

Scheme 6: Synthesis of compound **7**. a) NaN_3 (2 eq), H_2O, reflux, 21 h, 98%. b) Dess-Martin periodinane (1.3 eq), CH_2Cl_2, RT, 1 h, 88%. c) preQ$_1$ (1.1 eq), $(CH_3)_4NHB(OAc)_3$ (1.5 eq), HOAc, DMF, RT, 5 h, 37%.

6.1. 2-(2-Azidoethoxy)ethanol

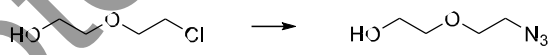

2-(2-Chloroethoxy)ethanol (8.47 ml, 80 mmol) was dissolved in ater (34 ml) and sodium azide (10.4 g, 160 mmol) was added. The reaction mixture was refluxed for 21 hours and then cooled to room temperature. The solution was extracted six times with 50 ml dichloromethane, dried over $MgSO_4$ and evaporated.

Yield: 10.3 g (98%) colourless oil

TLC (ethyl acetate/MeOH, 9:1): R_f = 0.60

^{1}H-NMR (300 MHz, $CDCl_3$): δ 2.37 (t, 1H, OH); 3.38 (t, 2H, H_2-C(2)); 3.58 (t, 2H, H_2-C(3)); 3.66 (t, 2H, H_2-C(4)); 3.69 - 3.75 (m, 2H, H_2-C(1)) ppm.

6.2. 2-(2-Azidoethoxy)acetaldehyde

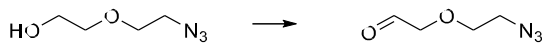

2-(2-Azidoethoxy)ethanol (337 mg, 2.57 mmol) was dissolved in dichloromethane (50 ml) and Dess-Martin periodinane (1.42 g, 3.34 mmol) was added portion wise. The solution was stirred at room temperature under argon for 1 hour, filtered through a celite pad and concentrated in vacuo. The crude product was purified by column chromatography on silica gel (diethyl ether/pentane, 1:2).

Yield: 293 mg (88%) colourless oil

TLC (diethyl ether /pentane, 1:2): R_f = 0.14

^{1}H-NMR (300 MHz, $CDCl_3$): δ 3.47 (t, 2H, H_2-C(3)); 3.74 (t, 2H, H_2-C(4)); 4.16 (s, 2H, H_2-C(2)); 9.73 (s, 1H, H-C(1)) ppm.

6.3. 7-((2-(2-Azidoethoxy)ethyl)aminomethyl)-7-deazaguanine trifluoroacetate 7

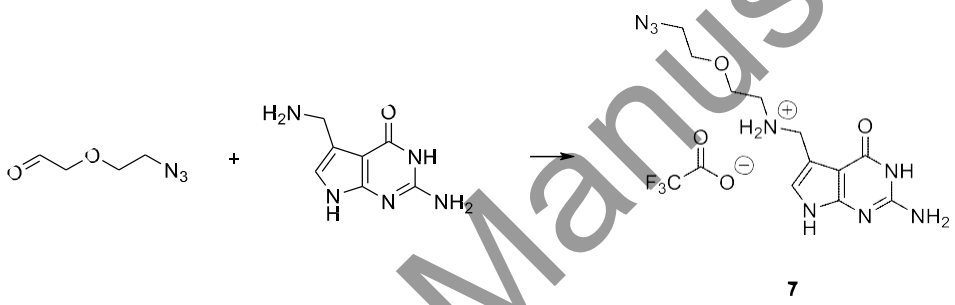

7

2-(2-Azidoetoxy)acetaldehyde (60 mg, 0.47 mmol) was dissolved in dimethylformamide (5 ml) and $preQ_1$ trifluoracetate (150 mg, 0.51 mmol) was added. Then tetramethylammonium triacetoxyborohydride (184 mg, 0.70 mmol) and acetic acid (30 µl) were added dropwise. The mixture was stirred at room temperature under argon for 5 hours, evaporated and dried under high vacuum. The crude product was purified by reversed phase chromatography on an ÄKTA prime plus system (LiChroprep® RP-18 (40 – 63 µm), 1% trifluoroacetic acid/acetonitrile, 100:0 – 70:30, 360 ml, flow rate 4 ml/min).

Yield: 69 mg (37%) of **7** as beige solid

ESI-MS (m/z): $[M+H]^+$ calculated: [293.15], found: [293.16]

^{1}H NMR (600 MHz, DMSO-d_6): δ 3.16 (t, 2H, H_2-C(1′)); 3.46 (t, 2H, H_2-C(4′)); 3.62 (t, 2H, H_2-C(3′)); 3.70 (t, 2H, H_2-C(2′)); 4.20 (t, 2H, H_2-C(7′)); 6.38 (s, 2H, H_2-N(2)); 6.82 (s, 1H, H-C(8)); 9.10 (s, 2H, H_2^+-N(7′)); 10.94 (s, 1H, H-N(1); 11.29 (s, 1H, H-N(9)) ppm.

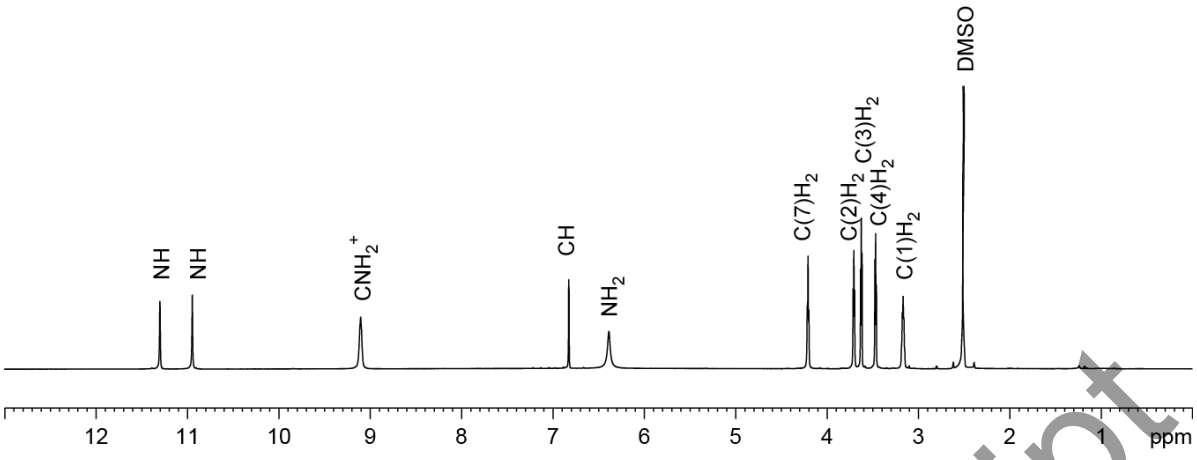

7. Synthesis of compound 8

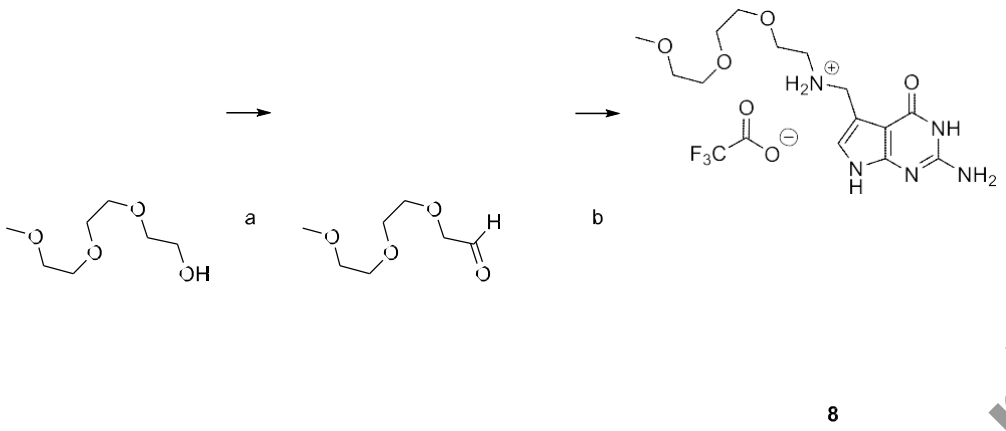

Scheme 7: Synthesis of compound **8**. a) Dess-Martin periodinane (1.15 eq), CH_2Cl_2, RT, 3 h, 73%. b) $preQ_1$ (1.1 eq), $(CH_3)_4NHB(OAc)_3$ (1.9 eq), HOAc, DMF, RT, 5 h, 21%.

7.1. 2-(2-(2-Methoxyethoxy)ethoxy)acetaldehyde

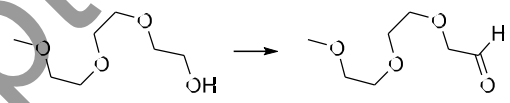

Dess-Martin periodinane (1000 mg, 2.35 mmol)was suspended in dry dichloromethane (20 ml) and triethylene glycol monomethyl ether (336 mg, 2.05 mmol) was added. The suspension was stirred at room temperature for 3 hours, filtered through a celite pad and evaporated.

Yield: 241 mg (73%)

^{1}H-NMR (300 MHz, d_6-DMSO): δ 3.38 (3H, H_3-C); 3.56 (t, 2H, H_2-C); 3.65 (t, 2H, H_2-C); 3.71 – 3.75 (m, 4H, H_2-C); 4.16 (2H, H_2-C(2)); 9.73 (1H, H-CO) ppm.

7.2. 7-(5,8,11-trioxa-2-azadodecyl)-7-deazaguanine trifluoroacetate 8

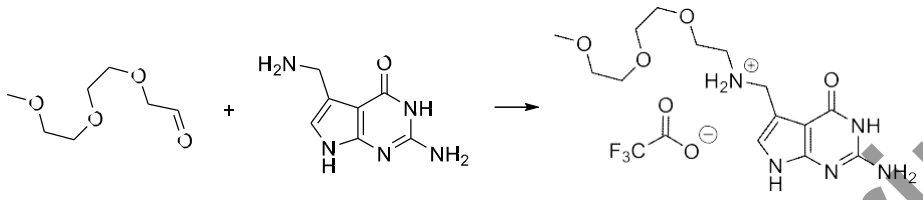

8

2-(2-(2-Methoxyethoxy)ethoxy)acetaldehyde (22 mg, 0.136 mmol) was dissolved in dry dimethylformamide (1 ml) and stirred at room temperature. Then, tetramethylammonium triacetoxyborohydride (66 mg, 0.253 mmol) and acetic acid (7 µl) were added successively. $PreQ_1$ trifluoroacetate (43 mg, 0.146 mmol) was dissolved in dry dimethylformamide (1 ml) and

was added dropwise to the reaction mixture. The solvents were evaporated after 5 hours and the crude product was purified by reversed phase column chromatography on an ÄKTA prime plus system (LiChroprep® RP-18 (40 – 63 µm), 1% trifluoroacetic acid/acetonitrile, 100:0 – 70:30, 360 ml, flow rate 4 ml/min).

Yield: 12.5 mg (21%) of **8** as yellow solid

HR-ESI-MS (m/z): $[M+H]^+$ calculated: [326.1823]; found: [326.1783]

^{1}H NMR (300 MHz, d_6-DMSO): δ 3.14 (2H, H_2-C); 3.23 (2H, H_2-C(7′)); 3.42 (2H, H_2-C); 3.52 (2H, H_2-C); 3.55 (5H, H_3-C, H_2-C); 3.66 (2H, H_2-C); 4.19 (2H, H_2-C); 6.31 (2H, H_2-N(2)); 6.82 (1H, H-C(8)); 9.01 (2H, H_2-N(7′)); 10.85 (1H, H-N(1)); 11.27 (1H, H-N(9)) ppm.

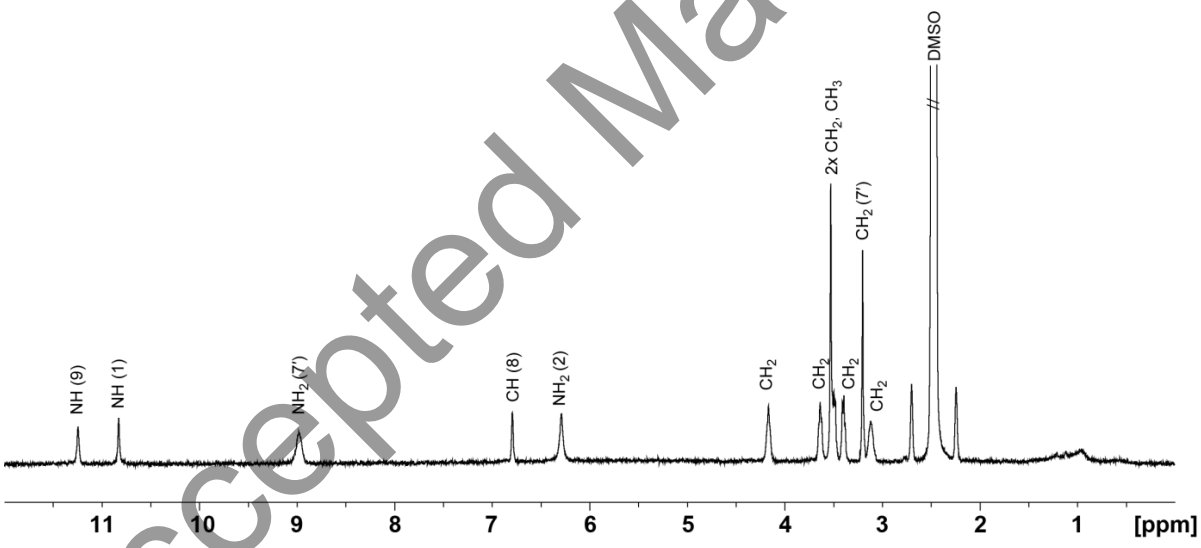

8. Synthesis of compound 9

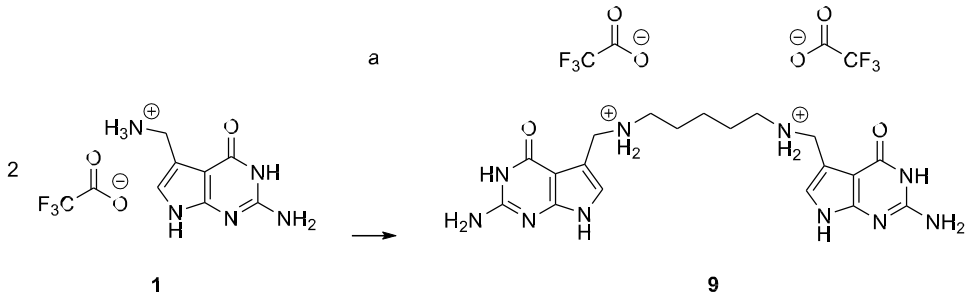

Scheme 8: Synthesis of compound **9**. a) glutaraldehyde (0.8 eq, 50wt%), $(CH_3)_4NHB(OAc)_3$ (3.2 eq), HOAc, DMF, RT, 4 h, 42%.

8.1. Pentyl-linked preQ$_1$ dimer 9

(2-(3-(2-amino-4-oxo-4,7-dihydro-3H-pyrrolo[2,3-d]pyrimidin-5-yl)propyl)isoindoline-1,3-dione) **9**

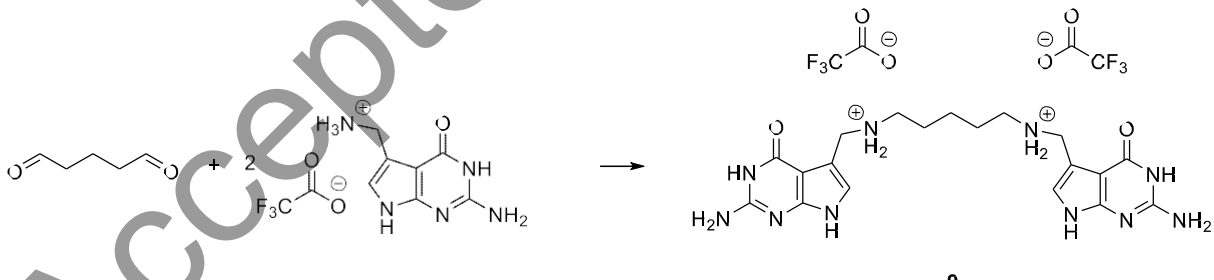

To a solution of preQ$_1$ trifluoroacetate (310 mg, 1.06 mmol) in dimethylformamide (5 ml), glutaraldehyde (84 mg, 50wt%, 0.423 mmol) was added. After the addition of tetramethylammonium triacetoxyborohydride (446 mg, 1.69 mmol) and acetic acid (114 µl) the orange solution was stirred for 4 hours at room temperature. The solvent was evaporated and the crude product was purified by reversed phase chromatography on an ÄKTA prime plus system (LiChroprep® RP-18 (40 – 63 µm), 1% trifluoroacetic acid/acetonitrile, 100:0 – 70:30, 480 ml, flow rate 4 ml/min).

Yield: 144 mg (42%) of **9** as white solid

TLC (RP, acetonitrile/water, 1:1): R_f = 0.68

ESI-MS (m/z): $[M+H]^+$ calculated: [427.48]; found: [427.30]

^{1}H NMR (300MHz, d_6-DMSO): δ 1.61 (m, 6H, H_2-C (2'-4'); 3.43 (m, 4H, H_2-C(1', 5')); 4.27 (s, 4H, H_2-C(7')); 6.34 (s, 4H, H_2-N(2)); 6.85 (s, 2H, H-C(8)); 9.68 (s, 4H, H_2 $^+$-N(7')); 10.79 (s, 2H, H-N); 11.36 (s, 2H, H-N) ppm.

9. Solid-phase synthesis of oligonucleotides

Oligoribonucleotides were synthesized by solid-phase RNA synthesis. Standard phosphoramidite chemistry using 2'-*O*-TOM or 2'-O-*t*BDMS ribonucleoside phosphoramidite building blocks (ChemGenes, Sigma Aldrich) and control pore glass (CPG) supports (ChemGenes, 1000 Å, 36.8 µmol/g) was applied (2,3). 2-Aminopurine nucleoside phosphoramidite was purchased from ChemGenes. All oligonucleotides were synthesized on ABI 392 or 394 Nucleic Acid Synthesizers following standard methods: detritylation (80 s) with dichloroacetic acid/1,2-dichloroethane (4/96); coupling (2.0 min) with phosphoramidites/acetonitrile (0.1 M x 130 µl) and benzylthiotetrazole/ acetonitrile (0.3 M × 360 µl); capping (3 × 0.4 min, Cap A/Cap B = 1/1) with Cap A: THF/phenoxyacetic anhydride (95/5) and Cap B: 10% 1-Methylimidazole in THF/sym-collidine (8/1); oxidation (1.0 min) with I_2 (20 mM) in THF/pyridine/H_2O (35/10/5). The solutions of amidites, tetrazole, and acetonitrile were dried over activated molecular sieves (3 Å) overnight.

10. Deprotection of oligonucleotides

The solid support was treated each with ammonium hydroxide (28-30%, 0.5 ml) and methylamine in water (40%, 0.5 ml) for 5 h at room temperature. The supernatant was removed and the solid support was washed 3 × with ethanol/water (1/1, v/v). The supernatant and washes were combined and evaporated to dryness. To remove the 2'-silyl protecting groups the resulting residue was treated with tetrabutylammonium fluoride trihydrate (TBAF·$3H_2O$) in THF (1 M, 2 ml) at 37°C overnight. The reaction was quenched by the addition of triethylammonium acetate (TEAA) (1 M, pH 7.4, 2 ml). The volume of the solution was reduced and the solution was desalted with a size exclusion column (GE Healthcare, HiPrep 26/10 Desalting; 2.6 × 10 cm; Sephadex G25) eluting with H_2O, the collected fraction was evaporated to dryness and dissolved in 1 ml H_2O. Analysis of the crude RNA after deprotection was performed by anion-exchange chromatography on a Dionex DNAPac PA-100 column (4 mm × 250 mm) at 80°C. Flow rate: 1 ml/min, eluant A: 25 mM Tris·HCl (pH 8.0), 6 M urea; eluant B: 25 mM Tris·HCl (pH 8.0), 0.5 M $NaClO_4$, 6 M urea; gradient: 0-60% B in A within 60 min, UV detection at 260 nm.

11. Purification of RNA

Crude RNA products were purified on a semipreparative Dionex DNAPac PA-100 column (9 mm × 250 mm) at 80°C with flow rate 2 ml/min. Fractions containing RNA were loaded on a C18 SepPak Plus cartridge (Waters/Millipore), washed with 0.1 M $(Et_3NH)^+HCO_3^-$, H_2O and

eluted with H_2O/CH_3CN (1/1). RNA containing fractions were lyophilized. Analysis of the quality of purified RNA was performed by anion-exchange chromatography with same conditions as for crude RNA. The molecular weight was confirmed by LC-ESI mass spectrometry. Yield determination was performed by UV photometrical analysis of oligonucleotide solutions.

12. Mass spectroscopy of RNA

All experiments were performed on a Finnigan LCQ Advantage MAX ion trap instrument connected to an Amersham Ettan micro LC system. RNA sequences were analyzed in the negative-ion mode with a potential of -4 kV applied to the spray needle. LC: Sample (200 pmol RNA dissolved in 30 µl of 20 mM EDTA solution; average injection volume: 30 µl); column (Waters XTerraMS, C18 2.5 µm; 1.0 × 50 mm) at 21°C; flow rate: 30 µl/min; eluant A: 8.6 mM TEA, 100 mM 1,1,1,3,3,3-hexafluoroisopropanol in H_2O (pH 8.0); eluant B: methanol; gradient: 0–100% B in A within 30 min; UV detection at 254 nm.

13. Determination of ligand binding affinities (K_D)

All fluorescence experiments were carried out on a Cary Eclipse spectrometer (Varian, Palo Alto, USA) equipped with a peltier block, a magnetic stirring device, and a RX2000 stopped-flow apparatus (Applied Photophysics Ltd., Leatherhead, UK). 2-Aminopurine labeled RNA samples (0.5 µM) were prepared in a total volume of 1000 µl of buffer (50 mM MOPS, 100 mM KCl, 2 mM $MgCl_2$, pH 7.5) (4). The samples were heated to 90°C for 2 minutes, allowed to cool to room temperature and held at 20°C in the peltier controlled sample holder in a quartz cuvette equipped with a small stir bar. Then, ligand was manually pipetted in 1µL aliquots in a way not to exceed a total volume increase of 2%. The solution was stirred during each titration step and allowed to equilibrate for at least 10 minutes before data collection. Spectra were recorded from 320 to 500 nm using the following instrumental parameters: excitation wavelength, 308 nm; increments, 1 nm; scan rate, 120 nm/min; slit widths, 10 nm. The apparent binding constants K_D were determined by following the increase in fluorescence after each titration step via integration of the area between 330 and 450 nm. Changes in fluorescence ($F - F_0$) were normalized to the maximum fluorescence measured in the absence of ligand. The

measurement for each titration step was repeated at least two times and the mean of the normalized fluorescence intensity was plotted against the ligand concentration. Data were fit using a K_D quadratic equation solution for 1:1 stoichiometry.

$$\frac{(F-F_0)}{(F_f-F_0)} = \frac{K_D+[RNA]_{total}+[ligand]_{total} - \sqrt{(K_D+[RNA]_{total}+[ligand]_{total})^2-4[RNA]_{total}[ligand]_{total}}}{2[RNA]_{total}}$$

F (fluorescence), F_0 (initial fluorescence), F_f (final fluorescence); $[RNA]_{total}$ (total concentration of RNA), $[ligand]_{total}$ (total concentration of added ligand for each titration step).

14. Determination of ligand binding kinetics (k_{obs} and k_{on})

Rate constants *k* for individual riboswitch variants were measured under pseudo-first-order conditions with ligand in excess over RNA (5). Stock solutions were prepared for each 2-aminopurine labeled RNA variant (concentration c_{RNA} = 0.6 µM in 50 mM MOPS pH 7.5, 100 mM KCl, 2 mM $MgCl_2$) and for each ligand (concentration c_{ligand} = 1.2 to 13.2 µM in 50 mM MOPS pH 7.5, 100 mM KCl, 2 mM $MgCl_2$). Mixing equal volumes of these stock solutions via the stopped-flow apparatus resulted in a final concentration of 0.3 µM RNA and of 0.6 to 6.6 µM ligand. Spectra were recorded at 20 °C using the following instrumental parameters: excitation wavelength, 308 nm; emission wavelength, 372 nm; increment of data point collection, 0.05 s; slit widths, 10 nm.

The stopped-flow fluorescence data were fit to a single-exponential equation:

$$F = A_1 + A_2 e^{-k't}$$

A_1 corresponds to final fluorescence; $A_2e^{-k't}$ corresponds to the change in fluorescence over time (t) at the observed rate k'. The measurement for each concentration was repeated at least two times and the mean of the observed rates k' was plotted against ligand concentration to obtain the rate constant k from the slope of the plot. The final rate constant *k* value is an arithmetic mean, determined from two independent stopped-flow measurements. All data processing was performed using *Kaleidagraph* software (Synergy Software, Reading, UK).

15. Cellular assays (IC_{50})

Synthetic class I and class II $preQ_1$ riboswitch encoding DNAs with *EcoR*I and *Sph*I overhangs were purchased from IDT (Integrated DNA Technologies) and cloned into *EcoR*I/*Sph*I sites of a pQE-70 bacterial expression vector (Qiagen) upstream to an eGFP reporter gene. Thus, the introduced riboswitch sequences replace the vector-encoded ribosomal binding site and provide the Shine-Dalgarno sequence required for translation. The plasmids were transformed

into $preQ_1$-deficient *E.coli* B105 cells (6). Bacterial cultures were grown to an OD_{600} of ~0.5 in LB medium (1% tryptone, 0.5% yeast extract, 0.5% NaCl, 10 mM $MgSO_4$, pH 7) before induction of reporter transcription by addition of 0.8 mM isopropyl-β-D-thiogalactopyranoside (IPTG). At the same time, ligands were added at different concentrations (0.1 µM – 7.5 mM). eGFP production was monitored by fluorescence measurement of 150 µl expression culture at 0 and 6 hours incubation using a Mithras LB 940 microplate reader (Berthold Technologies) and 96-well black clear bottom plates (Costar) with an excitation wavelength of 485 nm and an emission wavelength of 535 nm. The fluorescence intensities were corrected for background fluorescence of LB medium and normalized to the cell density determined at 600 nm. All data was log transformed and the IC_{50} value was determined with a fit to a four-parameter logistic equation.

$$Y = B + \frac{C - B}{1 + 10^{((789(:;<=))*?@77A78BC)}}$$

Y corresponds to % inhibition; B corresponds to the bottom plateau of % inhibition; C corresponds to the top plateau of % inhibition; X corresponds to the log of ligand concentration; HillSlope corresponds to the steepness of the curve; log(IC50) corresponds to the log of the half maximal inhibitory concentration. The final IC_{50} value was derived from at least two independent measurements. All data processing was performed using *GraphPad Prism 5* software (GraphPad Software, La Jolla, USA).

16. References

1. Bates,R.W.; Dewey,M.R., (2009) A formal synthesis of swainsonine by gold-catalyzed allene cyclization. *Org*. *Lett*., **11**, 3706–3708.

2. Micura,R. (2002) Small interfering RNAs and their chemical synthesis. *Angew. Chem. Int. Ed*., **41**, 2265–2269.

3. Pitsch,S., Weiss,P.A., Jenny,L., Stutz,A. and Wu,X. (2001) Reliable chemical synthesis of oligoribonucleotides (RNA) with 2′-O-[(triisopropylsilyl)oxy]methyl (2′-O-tom)-protected phosphoramidites. *Helv. Chim. Acta*, **84**, 3773–3795.

4. Rieder,R., Lang,K., Graber,D. and Micura,R. (2007) Ligand-induced folding of the adenosine deaminase A-riboswitch and implications on riboswitch translational control. *ChemBioChem*, **8**, 896–902.

5. Rieder,U., Kreutz,C. and Micura,R. (2010) Folding of a transcriptionally acting preQ$_1$ riboswitch. *Proc. Natl. Acad. Sci. U.S.A*., **107**, 10804–10809.

6. Gaur,R. and Varshney,U. (2005) Genetic analysis identifies a function for the queC (ybaX) gene product at an initial step in the queuosine biosynthetic pathway in Escherichia coli. *J. Bacteriol*., **187**, 6893–6901.

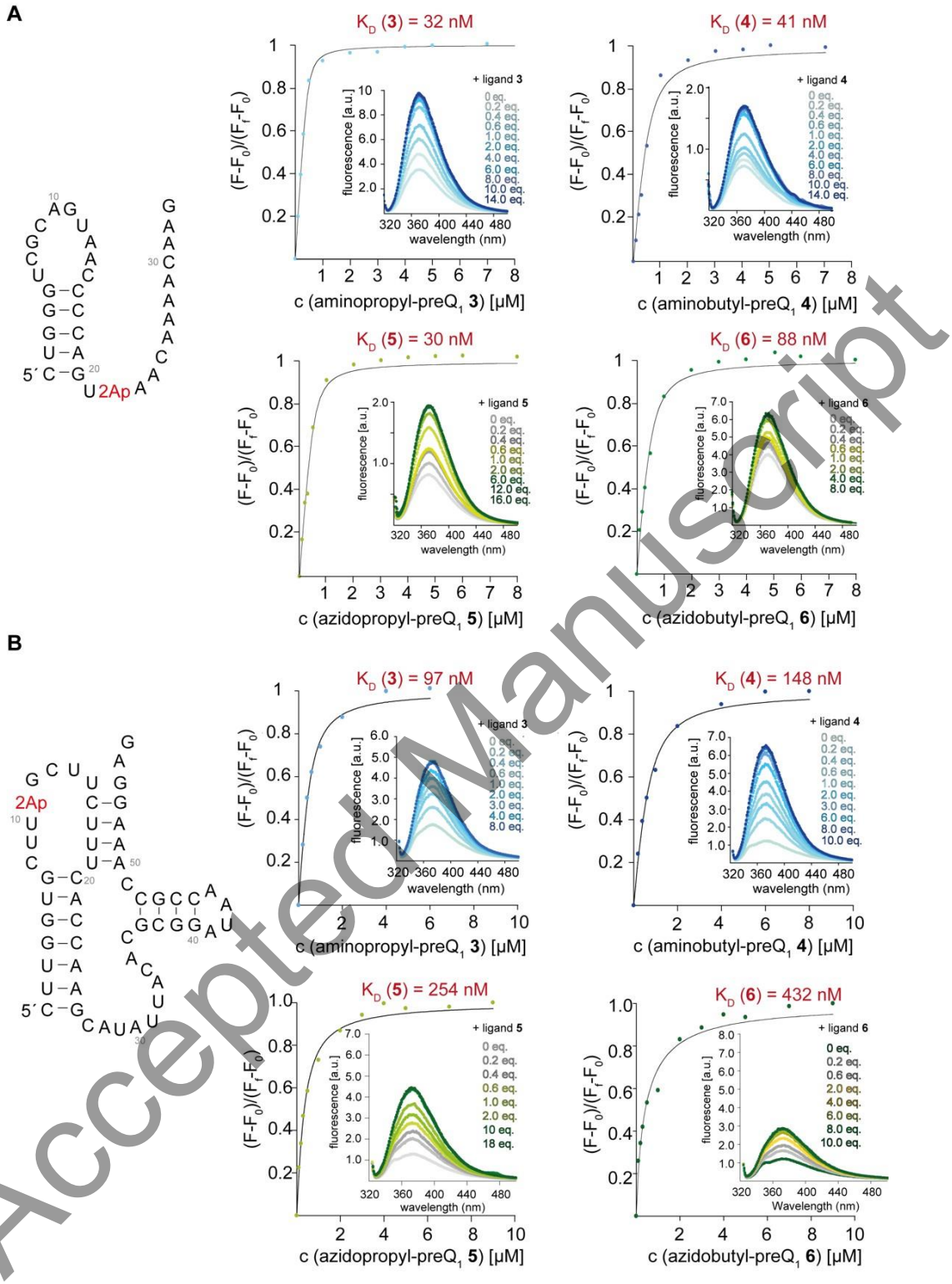

Supporting Figure S1. Fluorescence changes upon titration of preQ$_1$-I (U22Ap) (**A**) and preQ$_1$-II (A11Ap) (**B**) riboswitches with different concentrations of preQ$_1$ analogs (**3**, **4**, **5**, and **6**) for the determination of K_D-values. Normalized fluorescence intensities of the U22Ap variant were plotted as a function of preQ$_1$ concentrations. Changes in fluorescence (F-F$_0$) were normalized to the maximum fluorescence measured in saturating concentrations of preQ$_1$. The graph shows the best fit to a single-site binding model (see Supplementary Methods). The insets show fluorescence emission spectra (λ_{ex} = 308 nm) from 320 to 500 nm for each ligand concentration. For conditions see Supplementary Methods. For an overview of K_D-values of all ligand anaolgs investigated in this study see Tables 1 and 2.

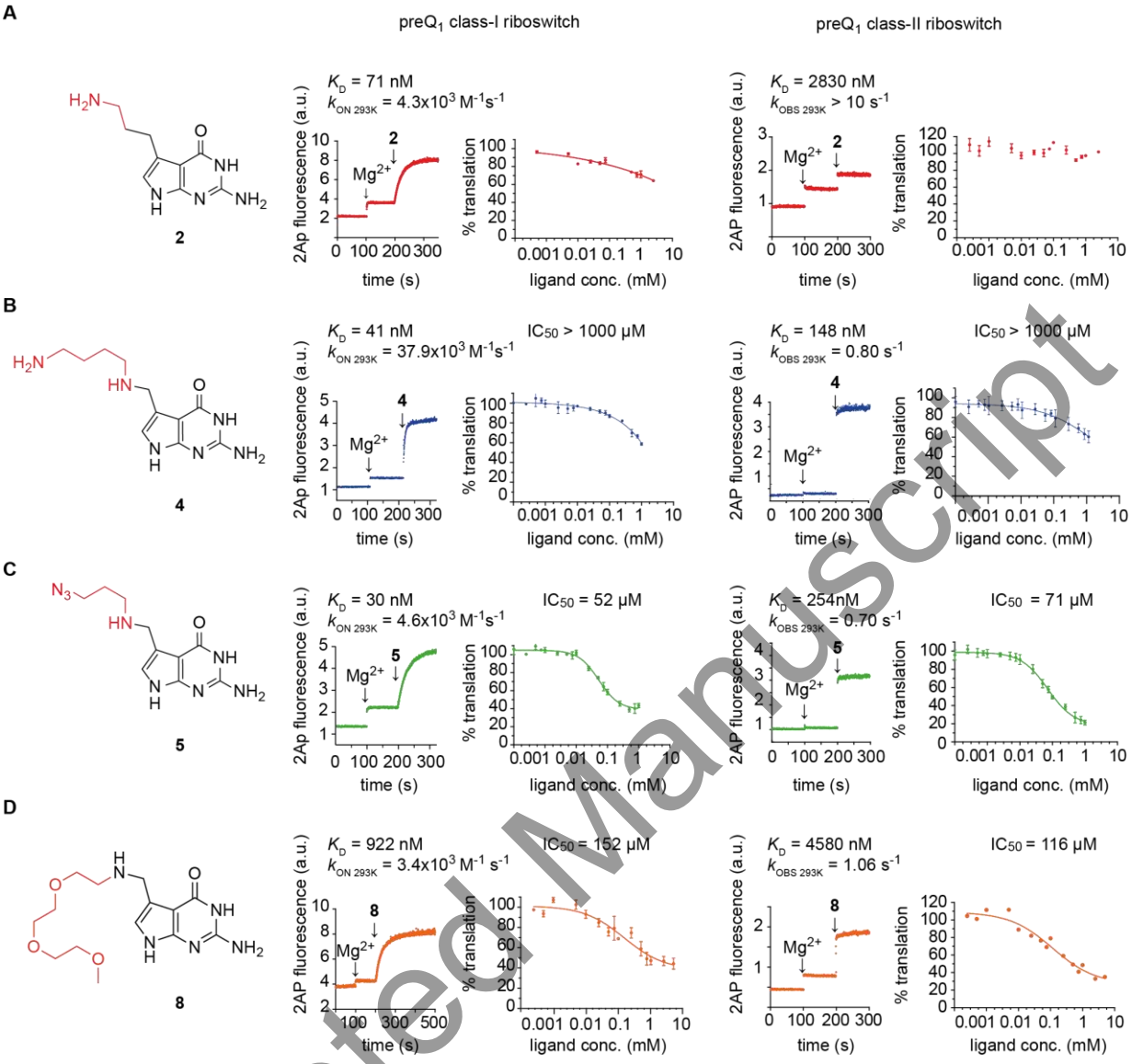

Supporting Figure S2. Comparison of *in vitro* and *in vivo* performance of preQ$_1$ class-I and -II riboswitches with modified ligand derivatives. **A**) Exemplary fluorescence time traces of Ap-labeled preQ$_1$ RNAs in response to Mg^{2+} and ligand analog **2** (conditions: 0.5 µM RNA, 100 mM KCl, 50 mM MOPS, pH 7.5, 293 K. Ligands: 2 mM $MgCl_2$, 5 µM compound **2**); affinities K_D were obtained from plots of normalized AP fluorescence intensities plotted as a function of ligand concentrations (for details see Supporting Figure S2); rate constants $k_{on(293)}$ of the *Tte* preQ$_1$ class-I riboswitch were obtained from plots of observed rates k_{obs} *vs* ligand concentrations (for details see Supporting Figure S3); binding to the *Spn* preQ$_1$-II riboswitch was independent of ligand concentration; for details of k_{obs} determination see Supporting Figure S4. Dose-dependent repression of gene expression: B105 *E. coli* cells transformed with constructs expressing eGFP under translational control of preQ$_1$ class-I and -II riboswitches were assayed for eGFP fluorescence in the presence of different preQ$_1$ **2** concentrations (0.10 µM to 5 mM). Data represent the mean of three biological replicates, with error bars indicating standard deviation. The data were fit with a four-parameter logistic function to derive the IC_{50} values as indicated. **B**) Same as (**A**), but for ligand derivative **4**. **C**) Same as (**A**), but for ligand derivative **5**. **D**) Same as (**A**), but for ligand derivative **8**.

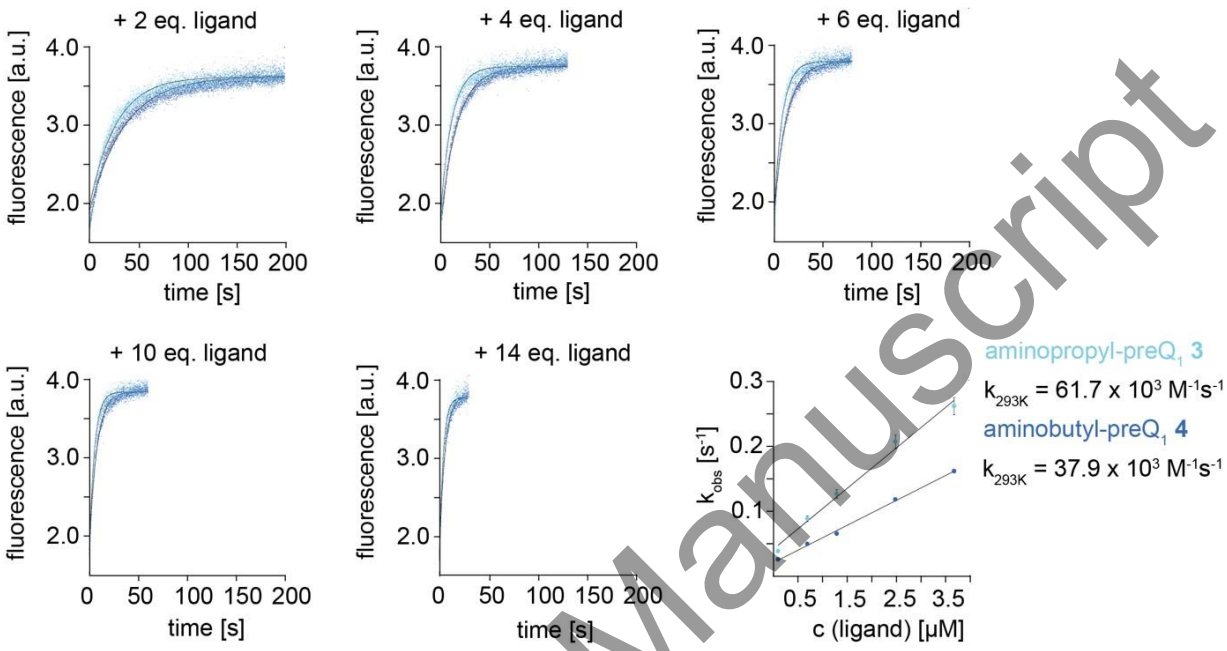

Supporting Figure S3. Stopped-flow fluorescence spectroscopy was used to monitor the kinetics of ligand preQ$_1$ binding to the *Tte* preQ$_1$ class-I riboswitch. Real time Ap fluorescence time traces of the *Tte* U22Ap variant at different concentrations of 3-aminopropyl- and 4-aminobutyl-modified preQ$_1$ **3** and **4** (solid line represents single-exponential curve fits); rate constants k_{293} from plots of observed rate k_{obs} versus ligand concentration (bottom right). c(RNA) = 0.3 µM, c($MgCl_2$) = 2 mM, 100 mM KCl, 50 mM MOPS, pH 7.5, 293 K. Ligand concentration c(ligand) as indicated.

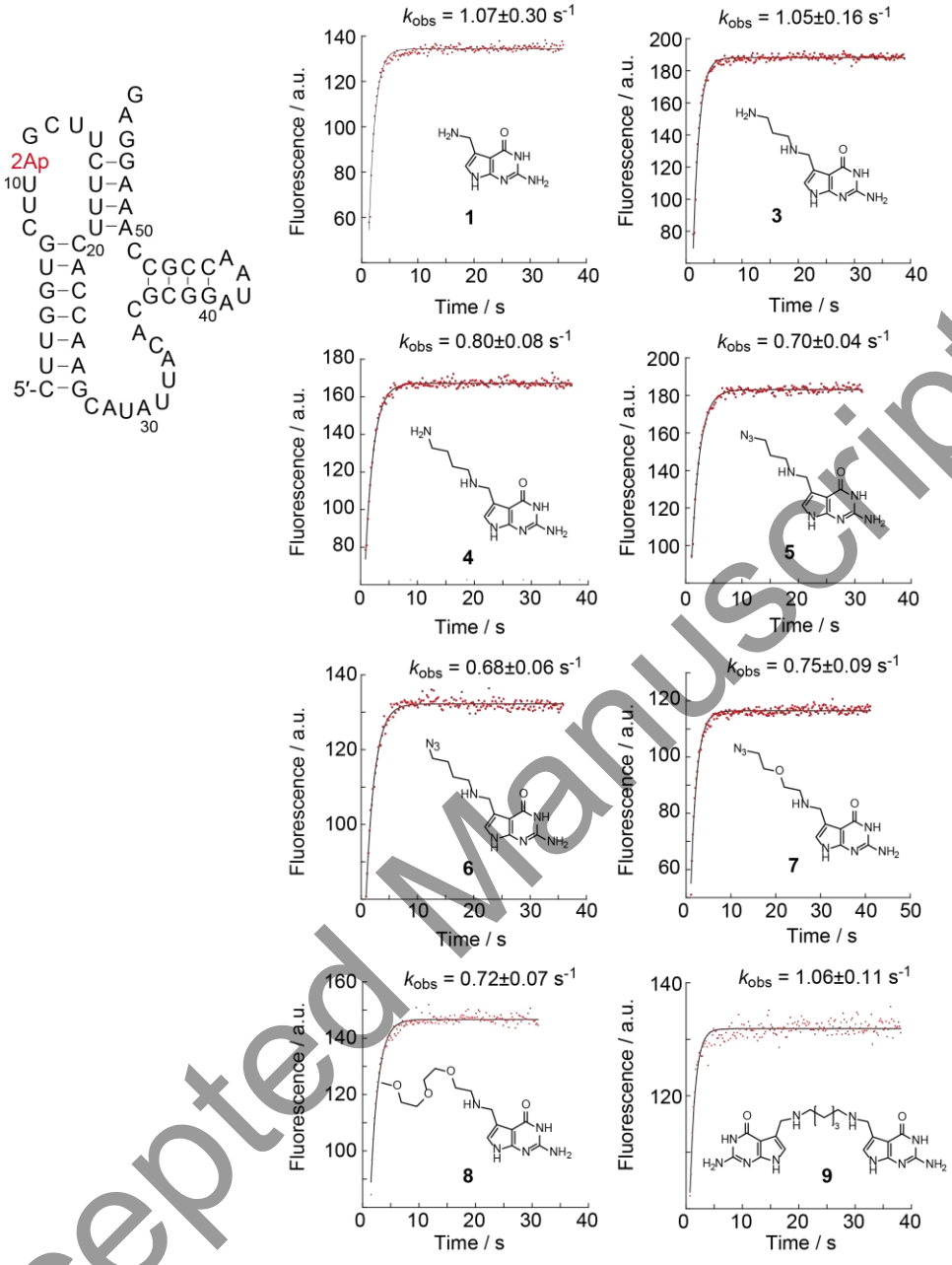

Supporting Figure S4. Stopped-flow fluorescence spectroscopy was used to monitor the kinetics of ligand preQ$_1$ binding to the *Spn* preQ$_1$ class-II riboswitch. Exemplary real time Ap fluorescence time traces of the *Spn* A11Ap variant in response to preQ$_1$ **1** and preQ$_1$ analogs **3** to **9** (solid line represents single-exponential curve fits); the observed rates k_{obs} were independent of ligand concentrations in the range tested (2 to 14-fold excess of ligand). c(RNA) = 0.3 µM, c($MgCl_2$) = 2 mM, 100 mM KCl, 50 mM MOPS, pH 7.5, 293 K. Ligand concentration c(ligand) = 1.8 µM.